Czech Technical University in Prague
Faculty of Electrical Engineering
Department of Electromagnetic Field

Design of volume clutter detection and parameter estimation algorithm

Diploma Thesis

Author: Bc. Karel Ročejdl
Supervisor: prof. Ing. František Vejražka, Csc.

−Assignment−

Abstract

Design of volume clutter detection and parameter estimation algorithm

Algorithms to detect clutter and to estimate its parameters play important role in radar systems. Once is clutter detected and its parameters estimated, radar can use such information to reject unwanted clutter signal and to extract information about target.

In this thesis *Detection and estimation algorithm* based on Doppler effect is designed to detect volume clutter and to estimate its Doppler frequency. Our algorithm is designed to allow efficient implementation in digital signal processor and its performance is compared with other algorithms available in literature. Designed algorithm is tested in various model situations and conditions to determine the most suitable detection parameters. Detection and estimation algorithm is then tested on real radar signal records. The main contribution of this thesis is design of new efficient algorithm to detect volume clutter and to estimate its radial velocity(Doppler frequency).

Key words

Doppler radar, Doppler frequency, volume clutter, clutter detection.

Abstrakt

Návrh algoritmu detekce a odhadu parametrů radarových odrazů od objemových útvarů

Algoritmy k rozpoznání přítomnosti objemových útvarů a určení jejich parametrů (Dopplerovské frekvence) hrají důležitou roli v radarových systémech. Pokud radar zná parametry objemových útvarů, může tyto informace použít k potlačení nechtěných odrazů.

V této práci je navržen algoritm pro detekci a určení Dopplerovské frekvence objemových útvarů. Algoritm je navržen aby umožňoval efektivní implementaci do signálového procesoru a jeho vlastnosti jsou porovnány s algoritmy dostupnými v literatuře. Poté je navržený algoritmus testován v různých modelových situacích a za různých podmínek, k určení optimálních parametrů algoritmu. Nakonec je algoritmus testován na reálných datech z radarových měření. Hlavní příspěvek této práce je návrh efektivního algoritmu pro detekci a určení parametrů objemových útvarů, jeho porovnání s dostupnými algoritmy v literatuře a následné ověření funkčnosti navrženého algoritmu na reálných datech.

Klíčová slova

Dopplerovský radar, Dopplerovská frekvence, detekce objemových útvarů.

Acknowledgement

I would like to thank to prof. Ing. František Vejražka, Csc. for useful advices and comments. I would like to express special thanks to Ing. Pavel Šedivý, Ph.D. for his endless support and encouragement, for his teaching and advices. Furthermore I would like to thank to company RETIA, a.s. for providing me real radar signal records.

At the end I want to thank to my family for never ending support through all the years.

Proclamation

I declare that this diploma thesis was written independently and only references stated herein were used according to "Methodical instruction about complying ethical principles during elaborating university theses".

In Prague on May 11th, 2015 .....

Contents

List of Abbreviations

AMTI	Adaptive Moving Target Indication
CPI	Coherent Processing Interval
CSR	Clutter to Signal Ratio
DFT	Digital Fourier Transform
DLC	Delay Line Cancellers
DSP	Digital Signal Processor
FFT	Fast Fourier Transform
LOS	Line of Sight
ML	Maximum Likelihood
MTD	Moving Target Detection
MTI	Moving Target Indication
PRF	Pulse Repetition Frequency
PRI	Pulse Repetition Interval
PPP	Pulse Pair Processing
RCS	Radar Cross Section
SCR	Signal to Clutter Ratio
SNR	Signal to Noise Ratio

List of Figures

List of Tables

Part I

Theoretical background

1 | Introduction to Radars

The word radar is abbreviation for "Radio Detection And Ranging". This perfectly describes main function of radar. Radar detects targets and measures their range or position by transmitting electromagnetic waves into space. However radar does not receive returns only from targets, but from other objects and even rain. Those unwanted returns are often stronger by several orders of magnitude, thus preventing target detection. One possible way to extract real targets from clutter background is to use examine different Doppler shifts between real target and unwanted clutter echoes.

In our thesis we will first establish radar theory and physics behind radar. Then we look at radar signal processing, how to deal with returned signal and how to extract information about target or clutter. Furthermore we design *Detection and estimation algorithm* to detect Doppler clutter signal and to estimate its parameters. We compare our algorithm to other methods available in literature. In the last part we test our detection algorithm on real data.

In this thesis we focus on primary, low PRF, Pulsed Doppler radar in air surveillance application.

1.1 Brief history

In 1888 German physicist Heinrich Hertz published his fundamental work "*About Radiation of Electrical Force*" for the Berlin Academy of Science. In this document Hertz described fundamental features of electromagnetic waves such as their propagation, polarisation, refraction and most importantly their capability of being reflected by metallic objects.

Christian Hülsmeyer is considered to be first Radar Engineer. Born in 1881 in northern Germany. He attended school in Bremen where he spent immense amount of time experimenting witch electromagnetic waves in laboratory. After ship accident, where his friend died, Hülsmeyer focused on idea to use electromagnetic waves reflections as warning system for ships. A year later he joined Siemens & Halske company. In 1904 Hülsmeyer (when he was only 22 years old) presented simple apparatus called *Telemobiloskop* which consisted of antenna, double spark and coherer. He managed to detect ships in range up to 3 kilometers. Unfortunately he did not manage to convince scientific and military society about importance of his discovery and later he had to terminate his research.

There was no public attention to radars until late twenties, however in early thirties radar potential was fully understood and in many countries (Germany, United Kingdom, USA etc.) begun rapid development, especially for military applications. During World War II development of radar systems escalated. Well described are early warning systems in east and south England and on German west frontier. During WWII were also constructed first airborne radars.

After World War II rapid development continued. Radar technology received public attention mainly in civil applications such as flight control and

ship navigation. Frequency band of 1−10GHz became widely accepted in radar community and is used until nowadays. In military applications radars had to solve more and more specialized tasks such as ballistic missile detection, missile navigation and even use in artillery.

With development in electronics and digital technology radars became high tech devices with complex structure and signal processing.

1.2 Types of radar

Since radar technology is used for various applications, there has always been development of new types of radars. We will note some of the major groups and characteristics.

Primary radar is the most classical application and widely known radar by public. Primary radar radiates electromagnetic waves which are reflected back from target and received by radar's antenna. From known speed of propagation and measured time delay between sent and received pulse we determine range of target.

Secondary radar. Target is equipped with *transponder*, which is device that detects radar's signal and with defined time delay sends message back to radar. Response is typically transmitted on different carrier frequency[2] Transmitted message usually contains additional informations such as GPS coordinates and flight identification number. Secondary radar requires cooperation with target, thus it is useful only in potentially friendly environment.

Monostatic radar has transmitter and receiver at the same place, very often they are integrated into one device. While *bistatic radar* has transmitter and receiver at different places, their distance can be even in order of kilometers. In such configuration we must ensure synchronization via conjoint link.

Active Radar radiates electromagnetic waves and receives waves reflected from target. While *Passive radar* doesn't transmit, passive radar only receives signals transmitted by target or signals transmitted by another source and reflected from target.

Continues Wave radar simultaneously transmits and receives signal. These systems are simpler and their maximum range is up to several tens of kilometres (but usually less).

Pulse Doppler Radar transmits pulses (or pulse train) and radar is repeatedly switching from transmitting mode to receiving mode. This design allows us to transmit higher mean power and thus achieve higher maximum range.

2 | Radar Theory

2.1 Range of target

In general, radar systems use modulated waveforms and directive antennas to transmit electromagnetic energy into space, or more precisely, into specific volume where we search for targets. Objects within search volume will reflect (scatter) portion of energy back to radar. These echoes are then received and processed by radar to obtain informations about targets. We are interested mainly in range, in its position in space, radial velocity and in more complex systems we are able to extract additional informations such as identity of target, target shape etc. Position of target in space is described in spherical coordinates by range R from radar, azimuth angle Φ and elevation angle Θ. Nevertheless we often also want to know radial velocity of target (obtained by Doppler shift in frequency) and then we search for target in four dimensional space.

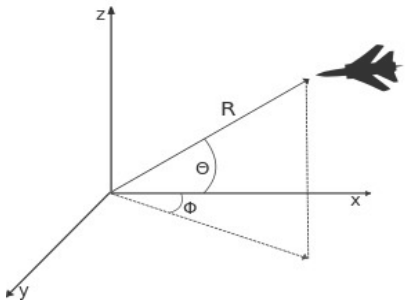

Figure 2.1: Spherical coordinate system used in radar systems

In pulse radar is range of target calculated by measuring time between sent pulse and received reflected (echo) pulse. In this case maximum range is determined, that time for pulse travelling towards target and back from the target must be less than time between two transmitted pulses (Pulse Repetition Interval, *PRI*). This is not rule, but we might have issues determining which returned pulse belongs to which transmitted pulse. In another words we can't distinguish if the returned pulse was reflected from target in way far range or in close range. This phenomenon is illustrated on figure 2.2. However we can improve our situation by using more complex techniques such as sending each pulse on different carrier frequency, using pulse modulation with different codes or changing pulse repetition interval (stagger).

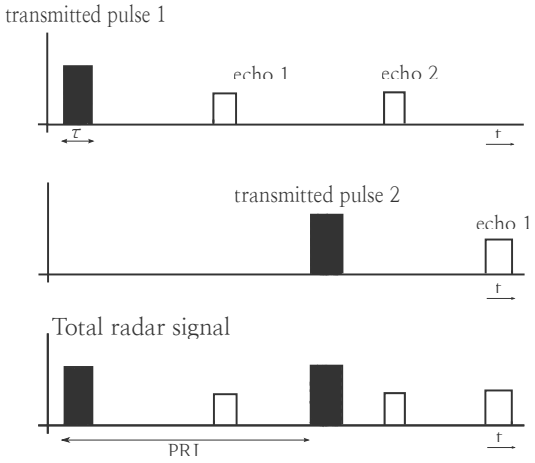

Figure 2.2: Pulse Repetition Interval and ambiguity caused by receiving pulse with travel time longer than PRI

Range of target can be calculated as

$$R = \frac{ct}{2} \tag{2.1}$$

where c is speed of light, t is measured time between transmitting and receiving pulse and factor two is there, because pulse has to travel way to and back from a target. Furthermore, in order to operate radar with maximum range R_{max} PRI must satisfy condition

$$PRI > \frac{2R_{max}}{c} \tag{2.2}$$

Another aspect in measuring range is how can we distinguish two targets in its close proximity, what is the minimum distance between objects to detect them as distinct objects? This minimum distance is called *range resolution* ΔR. Radar systems are designed to operate between minimum and maximum range, while this distance is divided into M range bins (*range resolution cells*), each of width ΔR . Targets separated by at least ΔR will be resolved in range. This is illustrated in figure 2.3. Then for range resolution ΔR we obtain simple formula (2.3).

$$\Delta R = \frac{c\tau}{2} = \frac{c}{2B} \tag{2.3}$$

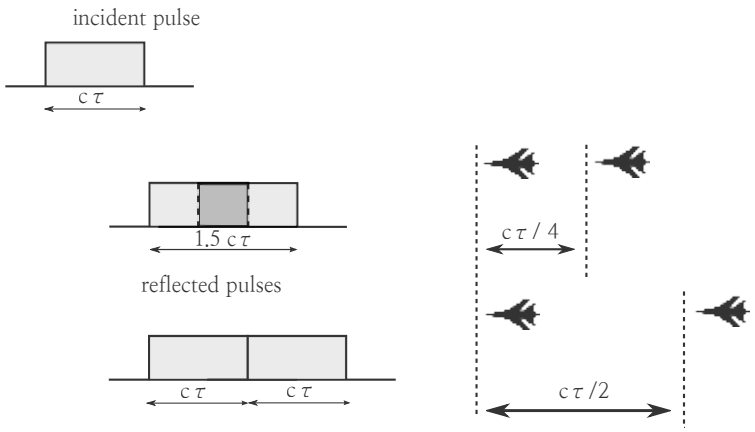

Figure 2.3: Illustration of required distance between two targets to be detected separately (i.e. range resolution)

2.2 Angle measurements

For measuring azimuth and elevation angle are used highly directional antennas. Directivity of antenna describes how much energy is focused by antenna into one direction, it is attribute describing radiated/received power with respect to angle of incidence[13]. This property can be very comfortably and graphically illustrated by antenna's radiation pattern. We are mostly interested in boresight (in main antenna beam), because that is where we extract target's angular position. Measuring of angle is done by steering antenna's main lobe (mechanically or electronically) through search space. During scan main lobe goes over target and, in ideal case, reflected (received) power will copy antenna's radiation pattern. According to maximum of received power we can estimate in which direction target is located.

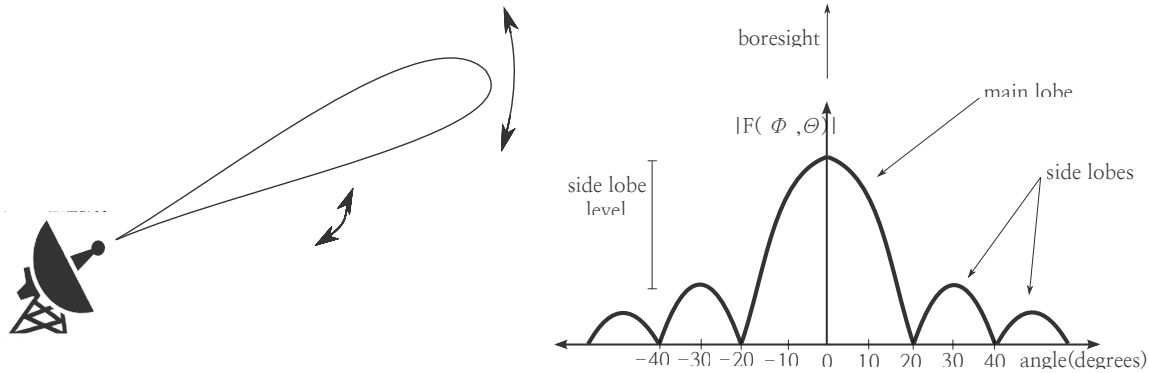

Figure 2.4: Steering of antenna's main lobe to conduct search through space. Antenna's radiation pattern

Directional antennas have typically very narrow beam. Width of very narrow pencil beam used in air surveillance radar is usually about 1° .

2.3 Radial velocity & Doppler effect

To measure radial velocity we can use two different approaches. The first, more intuitive, would be to measure position of target in space in two different time steps. From know travelled distance and known time we can easily calculate the velocity of target. However this approach can be very inaccurate since the error in determining target's position might be greater than actual travelled distance[2].

Second approach is to use so called Doppler effect, Doppler frequency, to obtain target's radial component of velocity. Doppler effect is shift in centre frequency of an incident waveform due to target's motion with respect to the source of radiation [3]. A waveform incident on target has equiphase wavefronts separated by wavelength λ. Target moving towards the source of radiation will force the reflected equiphase wavefronts to get closer to each other, leading to shorter wavelength, thus increasing frequency of received signal. Result is opposite while the target is moving away from source [3]. This phenomenon is illustrated in Figure 2.5.

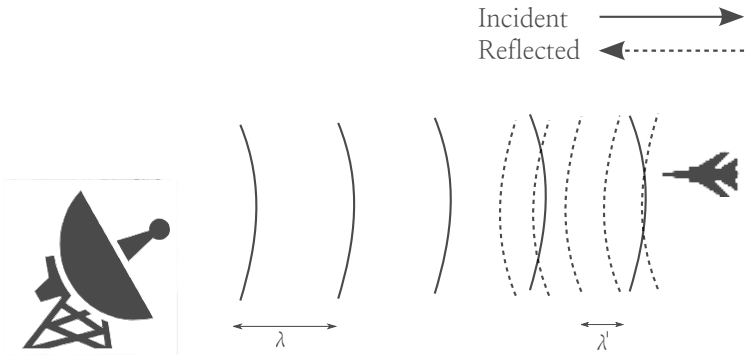

Figure 2.5: Change in wavelength (frequency) of reflected wave due to target's radial motion

The phase shift φ of radar signal on route to target and back can be expressed as

$$\varphi = \frac{2R \cdot 2\pi}{\lambda} \tag{2.5}$$

where R is range of target and λ is wavelength of transmitted signal. If the target has radial velocity

$$v_r = \frac{d(R)}{d(t)} \tag{2.6}$$

then phase changes are

$$\frac{d(\varphi)}{d(t)} = \frac{-4\pi \cdot v_r}{\lambda} \tag{2.7}$$

and this change in phase is equivalent to change in frequency – Doppler frequency

$$f_D = \frac{1}{2\pi}\frac{d(\varphi)}{d(t)} = \frac{-2v_r}{\lambda} \tag{2.8}$$

This principle is used in our Detection and estimation algorithm, because we use phase difference of successive samples to determine Doppler frequency.

Radar doesn't receive only echoes from target, but also echoes from all other objects in volume resolution cell and even from objects such as trees, vehicles and buildings. Magnitude of those unwanted signals might be several orders higher. Those unwanted echoes we call *clutter*. Doppler frequency analysis is used to detect targets in clutter environment. If our radar is stationary, echo from ground will have zero Doppler frequency, because there is no mutual movement. On other hand echo from for example aircraft will be shifted in frequency due to aircraft's motion.

In previous derivation we considered that radial velocity is equal to the target's own velocity. This, we might say, is rare occasion. Therefore for calculating Doppler frequency we can use more general formula

$$f_D = \frac{-2v_r}{\lambda}\cos\theta \tag{2.9}$$

where θ is angle between radar–target LOS and target's vector of motion.

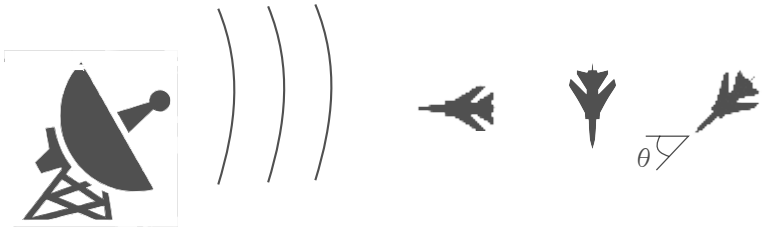

Figure 2.6: Different radial velocities

2.4 Range ambiguity – Doppler velocity ambiguity

Pulse Doppler radars are divide into three operational regimes according to Pulse Repetition Frequency (Table 2.1). Pulse Repetition Frequency is one of the critical parameters in design of radar system.

Table 2.1: Doppler velocity and range ambiguity according to PRF.

PRF	Unambiguous	
	Range	Velocity
Low	Yes	No
Medium	Yes	Yes
High	No	Yes

To improve unambiguous measurements we can implement several techniques. First technique used to help with unambiguous velocity measurements is use of multiple PRFs, called *stagger*. Stagger is examined more thoroughly in section 4.4.2. Other technique commonly used is *Pulse compression*. Pulse compression is frequency or phase modulation to widen signal bandwidth. Pulse compression is used, because we can transmit high energy with long pulse (range improvement) and simultaneously obtain resolution corresponding to a short pulse.

In our scenario radar is operating in low PRF regime.

2.5 Radar equation

Radar equation is relationship between transmitted and received power. Examining radar equation closely gives us insight into important radar parameters and overall design.

If we consider source which radiates into all directions equally (omni directional) and that radiated wave is spherical, then power density at any point in space (assuming a lossless propagation) is

$$S_1(R)=\frac{P_t}{4\pi R^2} \tag{2.10}$$

where P_t is power transmitted and R is distance.

Our incident wave induces surface current and target radiates electromagnetic energy into all directions. How much energy is radiated depends on target's size, orientation in space (angle of incidence) and physical properties. All those properties are summed up in *Radar Cross Section* σ of target (RCS itself is examined in section 2.6). We consider reflected electromagnetic wave to be spherical and in distance R the power density will be

$$S_2(R)=\frac{S_1\sigma}{4\pi R^2} \tag{2.11}$$

Thus total power received by radar is

$$P_r(R)=\frac{P_t\sigma}{(4\pi R^2)^2} \tag{2.12}$$

However radars in reality do not have omnidirectional antennas, actually we use antennas directive or even highly directive with pencil beams. This antenna's performance must be included into radar equation by using antenna's radiation pattern and its corresponding function $f(\Phi,\Theta)$ and antenna's gain G.

Furthermore actual power received by radar is also determined by *antenna's effective aperture* A_{eff}. Antenna's effective aperture is parameter describing relation between energy intercepted by antenna and incident electromagnetic

wave with certain power density S_2 [13].

$$P_r = A_{eff} f_p^2(\Phi,\Theta) S_2 \tag{2.13}$$

where A_{efp} is defines as

$$A_{eff} = \frac{\lambda^2}{4\pi} \tag{2.14}$$

And power received by radar P_r is

$$P_r(R,\Phi,\Theta) = \frac{P_t G_t G_r f_t^2(\Phi,\Theta) f_r^2(\Phi,\Theta) \sigma \lambda^2}{(4\pi)^3 R^4} \tag{2.15}$$

Another aspect which we have to consider in designing our radar system is propagation medium. Propagation medium, our atmosphere, is not lossless and power loss on signal's way from radar to target is characterized by attenuation L_{at}. While electromagnetic wave propagates in atmosphere it interacts with molecular and atomic structures, therefore transferring energy (which is absorbed and converted into heat mostly). Part of the energy is also scattered. This energy loss is attenuation loss and it is heavily dependent on wavelength. Attenuation caused by rain is additional element and is examined later.

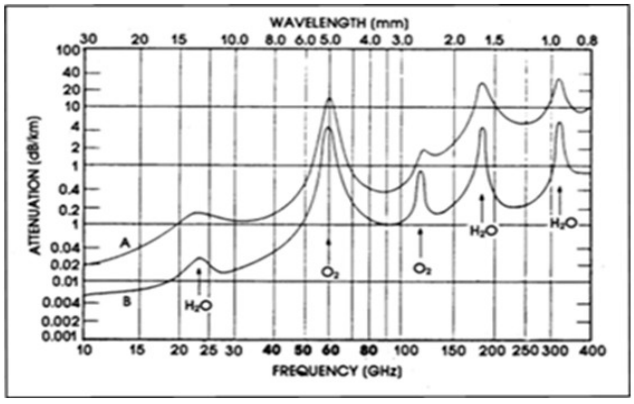

Figure 2.7: Attenuation in atmosphere. Curve A for altitude 4km above sea level. Curve B for sea level. Taken from [9]

Electromagnetic wave doesn't propagate only directly, but also bends in atmosphere and scatters (for example from ground), then the signal received is superposition of all. This is accounted in the *propagation factor* $F(\Theta)$. Final form of radar equation is

$$P_r(R,\Phi,\Theta) = \frac{P_t G_t G_r f_t^2(\Phi,\Theta) f_r^2(\Phi,\Theta) F^4(\Theta) \sigma \lambda^2}{(4\pi)^3 R^4 L_{at}^2} \tag{2.16}$$

2.6 Radar Cross Section

2.6.1 Definition

Incident electromagnetic wave on any object is scattered into all directions, therefore object becomes source of radiation, source of an echo signal. Radar transmits electromagnetic waves and then receives returned echoes. Thus would be very useful to quantify echo and its characteristics in terms of target parameters such as its size, shape, orientation in space etc. This quantifying parameter is *radar cross section* σ [m^2]. The RCS is cross-sectional area of metal sphere that would return the same echo signal as target. [1]

RCS of object is strongly dependent on incident wave's wavelength. If the wavelength is much greater than dimension of object, then this object will be only hardly detectable. On the other hand if object is much larger than incident wave's wavelength, then we achieve fine resolution and we can even see object in details.

2.6.2 Radar Cross Section of conducting sphere

In RCS calculations is conducting sphere considered to be the simplest object. Conducting sphere is, by nature, symmetrical thus reflected wave is co-polarized with the incident wave.

On figure 2.8 is shown RCS of conducting sphere as a function of its size, where $ka=2r\pi/\lambda$. This figure helps us explain different back scattering mechanisms, which are divided into 3 regions.

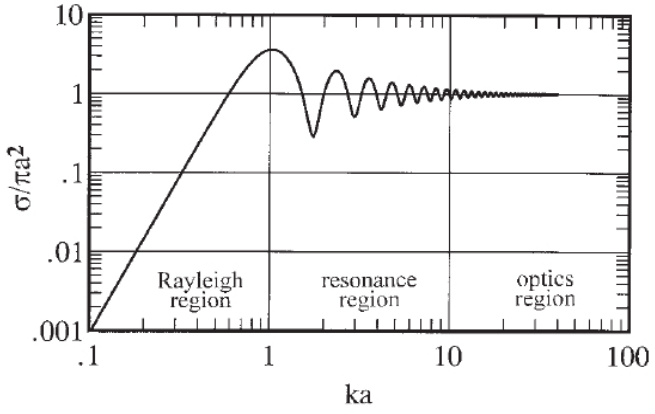

Figure 2.8: RCS plot of conducting sphere. Figure taken from Skolnik, M., *Radar Handbook*, 3rd Ed., McGraw-Hill, 2008 [1]

Rayleigh region, where typical body size is smaller than wavelength is determined by

$$\sigma = 9\pi r^2 \left(\frac{4\pi r}{\lambda}\right)^4 \tag{2.17}$$

where r is radius of sphere. This region is in our interest, because rain drops can be viewed as perfect small spheres. By look at formula (2.17) we see, that RCS of

raindrop will rapidly increase with radius.
In Resonance region is typical body size in interval roughly $\lambda - 3\lambda$. In optics region is λ smaller than size of target. Most of radar applications falls within optics region [3].

It is important to note that radar cross section doesn't resemble actual surface area of target, but it is quantity describing target's detectability. For example stealth aircrafts have RCS much smaller than its actual size.

Table 2.2: Example σ values at microwave frequencies

Target	Average σ [m^2]
Missile	0.5
Stealth aircraft	~0.1
Large fighter	6
Large military aircraft	40
Large civil aircraft	100

From[14]: Skolnik, M.I., *Introduction to Radar Systems*, 2nd Ed., McGraw–Hill, 1981.

Radar cross section of complicated objects and structures such as airplanes, vehicles, ships etc. is very difficult to calculate and so often they are experimentally measured. However those data are strictly classified.

2.6.3 Angle dependency

RCS is parameter quantifying reflectivity of target, it's not dependent on range. However, σ is heavily dependent on angle, because every reflected signal is superposition of reflected signals from each part of object, with complicated structure, therefore any minor change in angle can lead into huge change in RCS. This situation is illustrated on following figure.

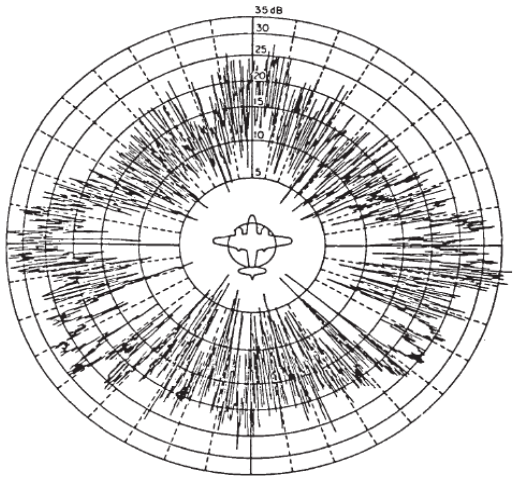

Figure 2.9: Example of fluctuating RCS for complicated objects (B–26 bomber). Figure taken from Skolnik, M., *Radar Handbook*, 3rd Ed., McGraw–Hill, 2008 [1]

In practice there is usually relative motion between radar and target. Thus RCS changes over time and there comes need to describe those changes. RCS can change in amplitude or in phase. Phase changes (fluctuations) are called *glint*. Radar estimates position of the target in its phase center, however due to glint the reflected wave might not be planar and therefore target's phase center could be determined outside actual target. The error in estimation target's position can be up to several meters. We can consider this error negligible except for special radar applications where high precision is required such as missile seekers.
RCS amplitude fluctuations depends on type of target. Types were defined by Swerling [10] and were divided into two groups – slow fluctuating and fast fluctuating. In this thesis we won't get into details, because it's not our point of interest, volume clutter changes very slowly.

2.7 Volume resolution cell

Volume illuminated by radar is dependent on range and for pencil beam we can use following equation [2]:

$$V = \frac{\pi}{4} R^2 \, \varphi_{3db} \theta_{3db} \Delta R \tag{2.19}$$

where R is distance between radar and volume resolution cell, φ_{3db} and θ_{3db} are beam widths in azimuth and elevation (rad), ΔR is range resolution.

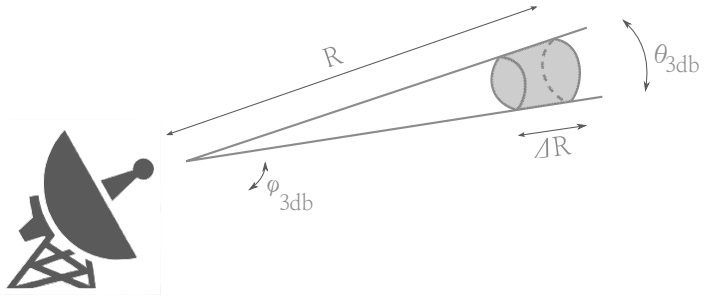

Figure 2.10: Volume resolution cell

2.8 Volume clutter

Volume clutter is general term that includes clutter (unwanted echoes) from chaff, weather and animals (birds, insects). Volume clutter is usually expressed as RCS per volume resolution cell. We will deal with Chaff in section 2.9, so now a few notes on clutter caused by weather are given.

2.8.1 RCS of precipitation

Raindrops can be considered as perfectly conducting small spheres. As was told in section 2.6.2 RCS of such a sphere is

$$\sigma = 9\pi r^2 \left(\frac{4\pi r}{\lambda}\right)^4 \qquad r \ll \lambda \tag{2.20}$$

where r is radius of raindrop.
Then we define RCS per resolution volume cell η, which is σ sum of all scatterers,

$$\eta = \sum_{i=1}^{N} \sigma_i \tag{2.21}$$

where N is number of scatterers in resolution cell.
Let's assume atmosphere with refraction index m, then RCS of raindrop can be approximated by

$$\sigma_i = \frac{\pi^5}{\alpha^4} K^2 D_i^6 \tag{2.22}$$

where D_i is i^{th} raindrop diameter and

$$K^2 = \left|\frac{m^2 - 1}{m^2 + 2}^2\right| \tag{2.23}$$

where m is complex refractive index following

$$m = n + ik \tag{2.24}$$

where n is refractive index and k absorption index.
Furthermore we define reflectivity factor Z (typically for resolution cell or unit volume)

$$Z = \sum_{i=1}^{N} D_i^6 \tag{2.25}$$

So we see that reflectivity and thus reflected power from rain is proportional to raindrop size (diameter). But to ease our calculations, we can use so called effective reflectivity Z_e. Z and Z_e are often treated equal (however that's incorrect). Effective reflectivity is relation between reflectivity and rainfall rate.

$$Z_e = a\, r^b \tag{2.26}$$

where r is rainfall rate (in $mm.h^{-1}$), a and b are empirical coefficients. Coefficients a and b are different for various geographical areas. For Europe are

mostly used a=200 and b=1.6 [7].
Another relation between reflectivity and precipitation can be shown in U.S. NEXRAD national weather radar system. The table commonly used for describing precipitation in meteorology is

Table 2.3: Relation between Rain Fall Rate and Reflectivity

Level	Rain Fall Rate [mm/hr]	Reflectivity [dBZ]	Category
1	0.49 to 2.7	18 to < 30	Light mist
2	2.7 to 13.3	30 to < 41	Moderate
3	13.3 to 27.3	41 to < 46	Heavy
4	27.3 to 48.6	46 to < 50	Very Heavy
5	48.6 to 133.2	50 to < 57	Intense
6	133.2 and greater	57 and above	Extreme

Table taken from[4]: Richards, M. A., Fundamentals of Radar Signal Processing, McGraw Hill 2005, ISBN: 0071444742

2.8.2 Precipitation Doppler spectrum

Ground clutter will have small frequency spread and will be concentrated around zero frequency (zero mean frequency) due to the fact, that there is no motion between stationary radar and ground. However this will not be the same for weather clutter. Rain clutter will be concentrated around mean frequency corresponding to raindrops fall velocity. This mean frequency is, as a rule, non zero. Situation is more complex, the shape of clutter Doppler spectra is determined by several mechanisms. According to [10] frequency spread of rain clutter depends on

- Wind shear. Wind velocity differs in various altitudes.
- Turbulences. Strong and random wind in particular area.
- Fall velocity distribution. Fall velocity of raindrops is not constant in whole rain area. Rain itself is not uniform either.
- Beam broadening

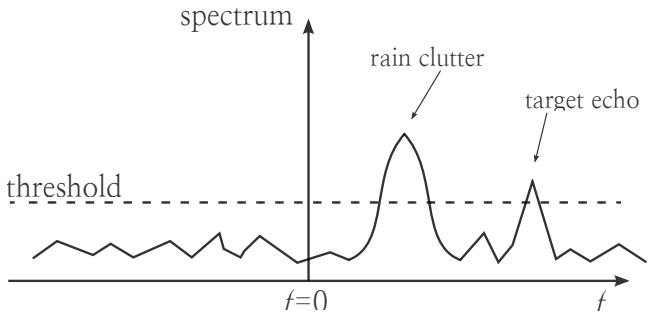

Figure 2.11: Doppler spectrum of received echo when clutter and target are present

For simple calculations it is custom to consider rain clutter power spectra as Gaussian-shaped [5][10].

2.9 Chaff

Chaff is electronic countermeasure (ECM) technique to combat enemy radar. It is huge amount of small dipoles cut in length of half the radar wavelength. Dipoles are made from very good conducting material and with size of half the wavelength they are great scatterers. Chaff released around into space by aircraft causes very strong echo signal, which will cover signal reflected from target. RCS is maximum, when dipole is in ideal position towards incident electromagnetic wave, which means to be perpendicular to direction of propagation and parallel to E plane [10]. Then RCS of single dipole is

$$\sigma_{max} = 0.857\,\lambda^2 \tag{2.27}$$

However, naturally, dipoles are usually made from lightweight materials, thus they are floating in the air and are randomly oriented. Therefore can be used approximation stated by [5]

$$\sigma = 0.18\,\lambda^2 N \tag{2.28}$$

where N is the total number of dipoles (typically per one volume resolution cell) and σ is RCS caused by that volume. It is fair to note, that in other publications the constant is slightly different.
Spectral characteristics are pretty much similar to that of rain and therefore we are not going to deal with chaff anymore. Relative motion caused by free fall is very small, because dipoles are very light and they float in the air. Thus dominant component for Doppler spectrum is wind shear and turbulences.

2.10 Meteorological objects

We can classify clouds according to several characteristics. For example we are interested in cloud's height level (altitude) and its lifetime. You may ask, why we are interested in clouds, but knowledge of clouds gives as additional informations, because different clouds appear in different heights, have different lifetime, transparency, reflectivity and different rain probability.
Atmosphere's vertical profile is divided into *floors*. For our geographical area it is

Table 2.4: Atmosphere division into floors.

Floor	Height
Top	5–13 km
Middle	2–7 km
Bottom	up to 2 km

Source: [7]

- *Convective clouds,* are clouds containing separate "cells" with high reflectivity. Lifetime is typically in tens of minutes
- *Layered clouds,* are homogeneous clouds with uniform reflectivity across large area. Their lifetime is typically in order of hours.

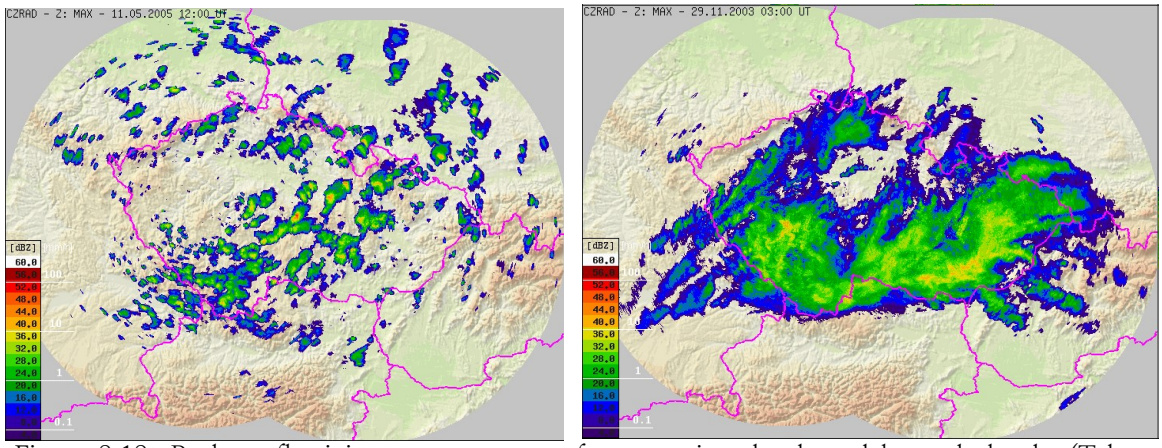

Figure 2.12: Radar reflectivity measurements of convective clouds and layered clouds. (Taken from [7])

3 | Radar block scheme

Radar consists of transmitter, receiver, signal processing unit and antenna. Transmitter, in our case represented by power amplifier, generates high power waveform that is radiated by antenna. In most cases are used short pulses so transmitter and receiver can share antenna together. This is accomplished by duplexer, which is device that allows strong signal from transmitter to propagate to antenna and weak received signal from antenna to propagate (in opposite direction) to receiver. Signal propagation from transmitter to receiver is blocked in order to prevent receiver from burning out. During transmission receiver is disconnected from antenna, thus it can not receive or process any signals.

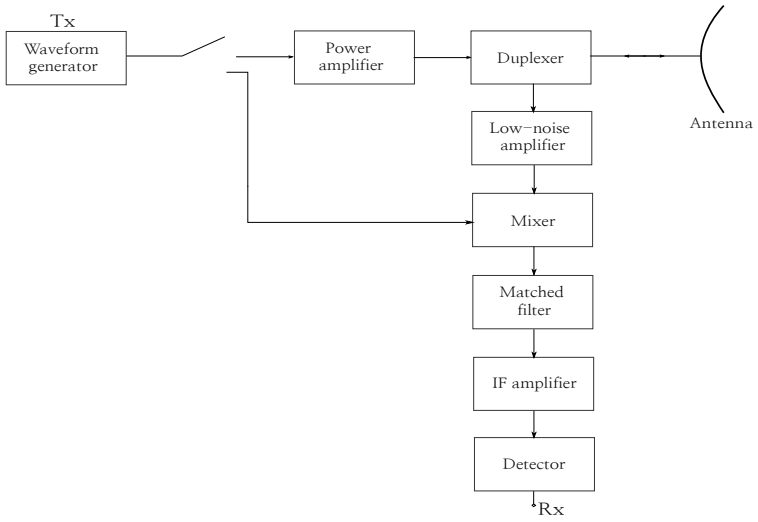

Figure 3.1: Primary radar block diagram

Received signal is amplified by low-noise amplifier. In such a system the noise level is important factor for radar performance, therefore low-noise amplifier is used in first stage, where it is the most critical. Following matched filter maximizes signal to noise ratio at its output. Afterwards we use MTI filter or Doppler filter to remove unwanted clutter signal from the useful signal. Resulting signal undergoes threshold test to determine, whether target is present or not.

The most of the signal processing is done over complex envelope of the received signal. In order to obtain *in-phase I* and *quadrature Q* components of complex envelope, we can use analog or digital approach. Since nowadays radars use digital signal processing extensively, digital approach is described.

3.1 Digital I/Q receiver

There is numerous different possibilities how to design digital I/Q receiver, so only one simple type with digital downconversion will be described.

Structure of the downconversion type is in Fig. 3.2. Incoming signal is

sampled by fast A/D converter with sampling frequency F_{sa}. Spectrum of digital signal is centered around its carrier frequency. Then is signal donwconverted into baseband by complex multiplication with reference signal. Downconversion (multiplication) creates unwanted replicas, which are eliminated by filter. At the end is sample rate reduced by decimation.

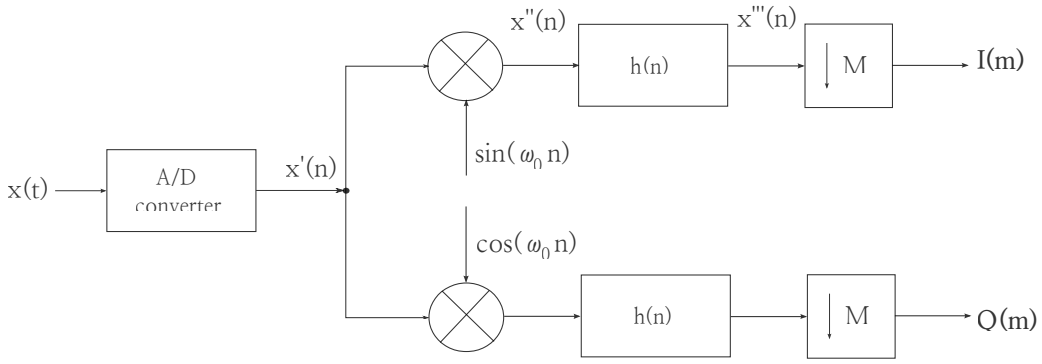

Figure 3.2: Structure of digital receiver with downconversion

To ease the burden of computational severity, we often improve the system in means of computational cost by using multirate processing and polyphase filters [6]. For purposes of our thesis complex samples are already provided and that's where detection algorithm begins.

4 | Doppler Processing

4.1 Data structure

Convenient way to access our signal data is to use matrix (or table) structure shown in Fig. 4.1. Let's consider that we transmit one pulse. As electromagnetic wave propagates through the space, energy is scattered back from intercepted objects. After the transmission of pulse, coherent receiver is receiving echo signal. The received signal is processed by I/Q demodulator as was explained above. The resulting signal is then sampled, while samples (echoes) from on pulse are organized into vector and they are representing *range bins* or *range cells*[+] . Each particular element of the matrix is complex number range sample having real and imaginary (I and Q) components

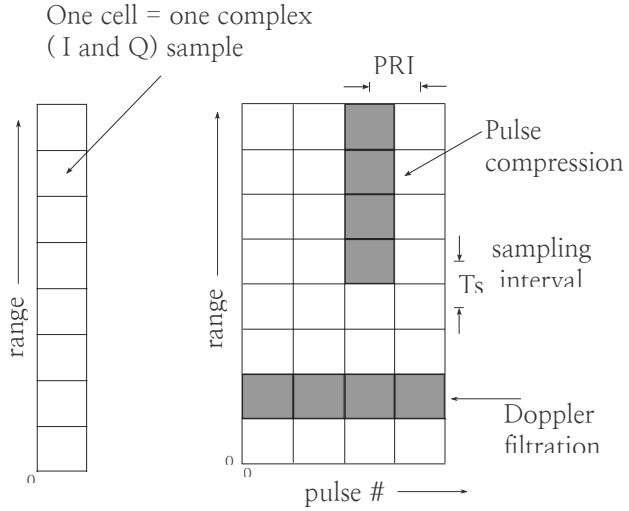

Fig. 4.1: Organized data structure of received radar signal samples for signal processing. Vector of samples for one pulse and matrix of samples for one CPI

However usually radar doesn't transmit just one pulse but a series of pulses, often called *burst* or *pulse train*. The time T between transmission of subsequent pulses is *pulse repetition interval* (PRI). Vectors of samples from several following pulses are organized into matrix (or table). The time needed to obtain this data is number of pulses multiplied by T, and if those pulses were coherent, then we are speaking about *coherent processing interval* (CPI). In most cases, one CPI is collected while using constant radar frequency, constants PRI and same pulse waveform for pulses [4].

We can use in advantage the way our samples are organized. The samples in one row are samples from the same resolution bin, they are samples with same delay from transmitted pulse, they are echoes from one region but in different time, measured with sampling interval corresponding to PRF.

[+] We have to be careful with using other terms as *resolution bins* and *resolution cells*, because these may be interpreted as range bins and range cells. Sampling interval in range doesn't have to be equal to range resolution.

Doppler processing is based on coherence of transmitted and received signal. For Doppler processing we are using samples received with delay corresponding to PRI from the same range bin. Phase difference between transmitted and received signal remains constant over samples from same range bin if the target inside that range bin is motionless. If the target is moving†, then we can observe change of phase difference (distance change) due to phase delay produced by propagation of signal towards the target and back.

Based on Doppler processing, were developed several techniques to combat unwanted clutter echoes. The most common ones are

- *Moving Target Indication* (MTI)
- *Adaptive Moving Target Indication* (AMTI)
- *Moving Target Detection* (MTD).

4.2 Moving Target Indication (MTI)

Moving Target Indication (MTI) is historically first and the simplest technique to combat unwanted clutter. We assume that our radar is stationary and the clutter background is completely motionless†. In such a scenario, the clutter Doppler spectrum is centered at zero Doppler frequency. Thus we can use simple high−pass filter to eliminate clutter spectrum.

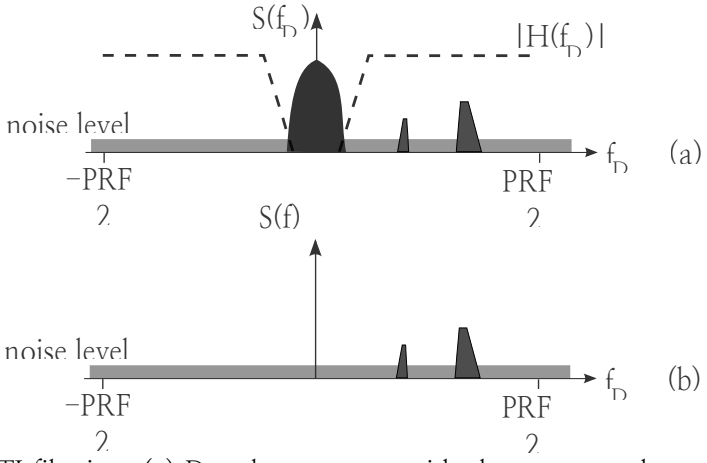

Figure 4.2: MTI filtering: (a) Doppler spectrum with clutter centered at zero Doppler frequency and MTI filter frequency response, (b) Doppler spectrum after filtration − only targets echo signals left

† For simplicity we consider scenario, when the target doesn't leave range resolution cell because of its motion.

To process our data we take from our data matrix (Fig. 4.1) one row, which is a vector of complex samples from same range bin. This vector will be fed as an input to MTI filter. As an output we will obtain signal with noise and target signal components. This will be passed to threshold detector to undergo detection test. MTI processing has disadvantage, that after detection we get information only about if there is target present or not. However we don't know what is target's radial velocity or how many targets are actually present in particular range bin.

Commonly used in MTI design are *pulse cancellers*. The two-pulse MTI canceller shown on Fig. 4.3 works as a subtractor, which subtracts echoes from successive pairs of pulses. Basic idea behind the pulse canceller is, that if radar illuminate stationary targets (buildings, ground etc.), then their echo pulses will remain same over time. Thus following pulses will cancel out completely in subtractor (delay line canceller, DLC) and we will obtain zero output. However if target will be in motion, then successive pulses will be received with different phase and their subtraction will have non zero result.

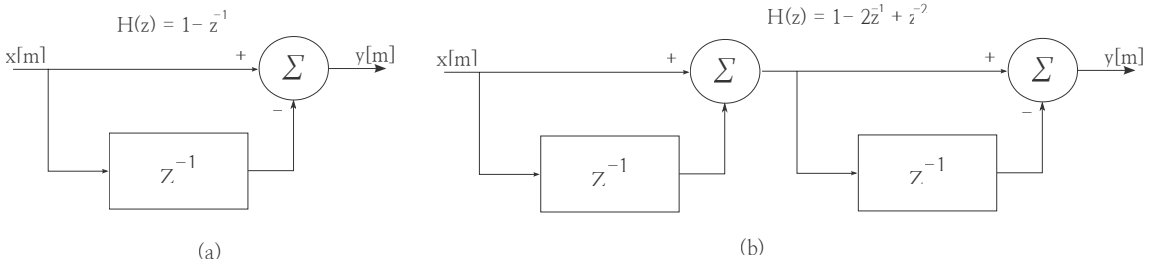

Figure 4.3: (a) single delay line canceller and (b) double delay line canceller.

Magnitude of the frequency response is shown in Fig 4.4. Our main stress is that gain over the passband interval is non-uniform, peaking at Doppler frequency of half the PRF. Different spectral components representing different radial velocities corresponding to different Doppler frequencies will be amplified and or attenuated.

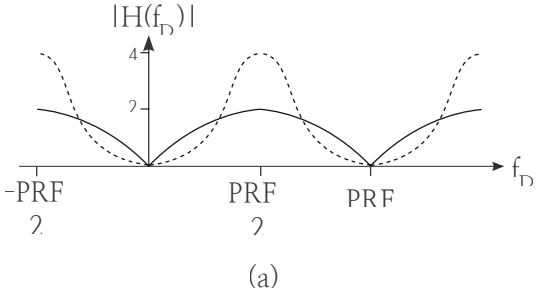

Figure 4.4: Magnitude of frequency response: solid line is single delay line canceller and dashed line is double delay line canceller

† These are not ultimate conditions, we can as well consider scenario, where radar platform is in motion. However, in such a case we need , from knowledge of radar's movement and geometry, to shift the clutter spectrum to zero frequency first.

From frequency characteristic in Fig. 4.4 we see that targets with Doppler frequencies around multiples of PRF will not be detected (blind speeds). This issue can be resolved by use of stagger.

4.3 Adaptive MTI (AMTI)

Adaptive Moving Target Indication (AMTI) allows Doppler processing to reject clutters not only from "stationary" ground clutter, but other clutters such as weather volume clutter as well. In general we use Adaptive MTI in situations, where we except more clutter sources with different radial velocities. For example volume clutter (precipitation) changes its Doppler spectrum signature over time (change of wind speed and direction), so there raises a need to adapt our clutter rejection frequency band to combat changes in environment. Again we can find many different analog and digital realization of AMTI, so we will mention one basic approach described in [2].

To design AMTI we can use cascade of two stop-band filters. First filter with $H_g(f)$ is set up around zero Doppler frequency to reject ground clutter, as was in previous case with ordinary MTI. Second filer with $H_v(f)$ is adaptively changed to reject frequency band, where variable clutter is positioned. Disadvantage of this realization is, that we increase passband ripple and decrease transition.

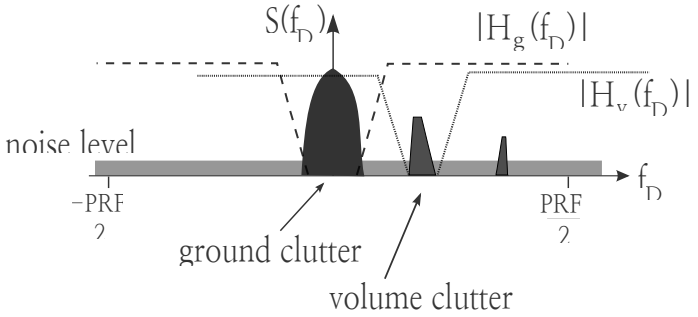

Figure 4.5: Doppler spectrum with ground and volume clutters. Amplitude frequency characteristic $H_g(f)$ to reject ground clutter and $H_v(f)$ to reject volume clutter

4.4 Moving Target Detection

Moving Target Detection (MTD) is the most advanced Doppler processing technique for detection of moving targets. MTD is used primarily in Pulse Doppler radars. We are using spectral analysis (*fast Fourier Transform*) of signal (samples) from one range bin. Samples over time from one range bin are declared as a signal, that enters bank of bandpass filters, which can reject clutter spectra. Change in phase of several following pulses introduces Doppler shift.

4.4.1 Bank of filters and DFT

Bank of bandpass filters is realized digitally by Fast Fourier Transform (FFT) or by bank of transversal filters. Filter performance can be improved by weighting filter coefficients or input samples. Most considerable parameter in filter design for our bank of filters is sidelobes separation, which can be

minimized by use of windows (weighting). Signal from the filter output then undergoes threshold test to decide if there is target present. Because of use of the bank of filters, we can determine not only if there is target present, but as well its approximate radial velocity (corresponding to the filter) and in case that there are more targets we can distinguish between them, as long as they are separate enough in Doppler frequencies.

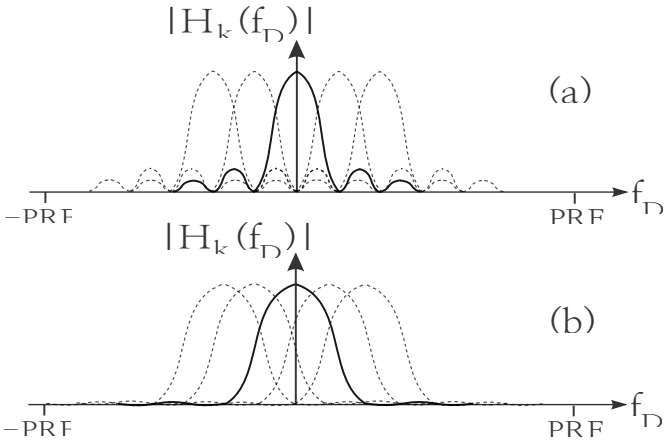

Figure 4.6: Magnitude of frequency characteristic of bank of Doppler filters: (a) no window (b) with application of window

Number of Doppler filters is usually chosen equal to number of pulses processed [5]. Filters are designed equidistantly over the −PRF to PRF Doppler frequency base band. The bandwidth of the Doppler filter in general determines the Doppler resolution. Because we are using separate narrowband filters (and noise level is proportional to the frequency band processed by the filter), we are achieving better SNR at the output of the each filter and so better detection performance.

Reader may notice that Doppler filters are overlapping, which means that target can be detected in two neighbouring filters. However target signals from those two filters will most likely have different amplitudes, which can actually be used for finer estimation of target's radial velocity by comparing output amplitudes. Their ratio (i.e. weight) corresponds to more precise estimate, as long as is Doppler resolution precise enough, or we can use interpolation techniques described for example in [4].

Modern radar systems with digital Doppler signal processing employ bank of bandpass filters via Discrete Fourier Transform (and it's effective equivalent Fast Fourier Transform FFT). This approach has significant advantages. DFT from input data vector (same range bin samples) creates k−point spectral analysis. Each of the k spectral points represents matched filter with a *sinc* function, tuned to a different Doppler frequency. Thus DFT creates bank of K bandpass filters equidistantly spaced in frequencies and centered at integer multiples of PRF/K

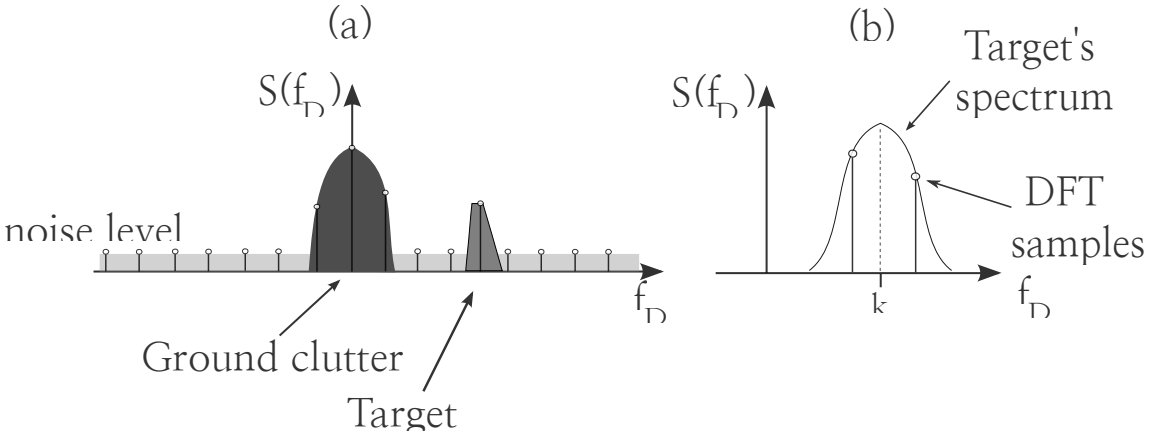

Figure 4.7: (a) FFT used to calculate signal spectrum, (b) mismatch of Doppler filter and target's spectrum

We can adjust our bank of filters to new situation by changing the number of bandpass filters (number of spectral points k, size of DFT) as well as by changing filter shape of filters by weighting input samples with a window.

FFT approach is used in Quadratic Interpolation around DFT peak algorithm (section 7) as comparison to our designed detection and estimation algorithm.

4.4.2 Stagger

PRF staggering is technique used to combat an effect of blind speeds and to prevent jamming. Blind speeds are introduced to our system via Pulse Repetition Frequency (PRF). Stationary clutter centered around zero Doppler frequency has its images at integer multiples of PRF (Fig.X.X), and thus any echo signal received from target with radial velocity corresponding to the PRF in Doppler frequencies, will not be detected. Blind speeds can be calculated as

$$v_b = \frac{\lambda}{2T} = k\frac{c}{2}\frac{PRF}{f_{carrier}} \tag{4.1}$$

where λ is wavelength of transmitted pulse, k is number of blind speed and T is Pulse Repetition Interval (PRI).

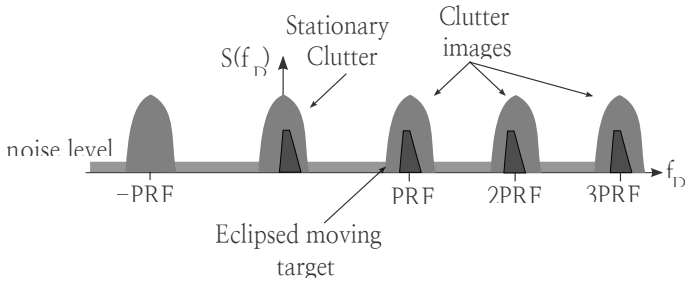

Figure 4.8: Demonstration of clutter bend over principle and creation of blind speeds at the integer multiples of PRF

PRF staggering is changing Pulse Repetition Interval, because different PRF results in different blind speeds. With different PRF we can detect target signals that would otherwise be eclipsed by strong clutter signal.

PRF staggering can be used in pulse–to–pulse basis or CPI–to–CPI.

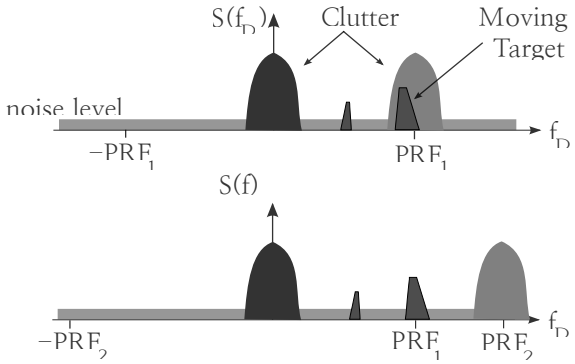

Figure 4.9: The use of two PRFs to avoid blind speeds. In upper figure is target's echo signal eclipsed by strong echo signal, while at the lower figure is the clutter signal shifted to different Doppler frequency, because of different PRF

It is much more challenging to build a stable transmitter for pulse–to–pulse operation, than it is for the other (scan–to–scan) case. Pulse–to–pulse staggering is preferable with MTI processing, while dwell–to–dwell staggering is commonly used with filter bank processing [1]. Staggering is usually described with PRI_1 / PRI_2 ratio and optimal stagger ratio is chosen according to desired velocity range without blind speeds.

Disadvantage of PRF staggering is, that transmission of several CPIs represents significant amount of radar's operational time and energy [4]. PRF staggering modifies the passband shape of the MTI filter [5] in a negative way.

Our detection and estimation algorithm uses constant single PRF. However one scenario with multiple pulse–to–pulse PRI's is simulated to examine effect of stagger on our detection and estimation algorithm.

Part II

Model, algorithms and scenarios

Core of our interest is to estimate radial velocity component (i.e. Doppler frequency) of Doppler clutter signal. This information is needed for volume clutter suppression synthesis.

Several ways to estimate mean Doppler frequency are simulated and their performance compared in our simulations. Thorough performance analysis of Detection and estimation algorithm is done to determine optimal algorithm parameters. Test on real data (records of radar signal) is performed to confirm Detection and estimation algorithm accuracy.

5 | Simulation model

In simulation model we generate target Doppler signal and clutter Doppler signal in noise environment. Our detection and estimation algorithm is tested on model situation and then compared to other methods available in literature [4] (such as Quadratic Interpolation and Pulse Pair Processing). Detection and estimation algorithm's performance is investigated in various scenarios in different conditions. Each situation is simulated multiple times to obtain credible results. We are mainly interested in detection and estimation accuracy with respect to different levels of SNR and size of resolution cell.

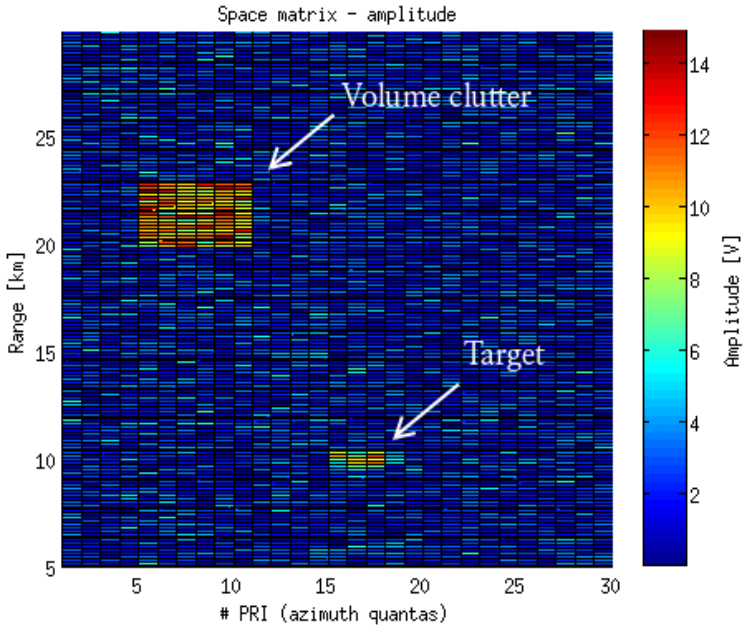

Figure 5.1: Matrix of complex samples representing noise environment with target and volume clutter Doppler signals. (SNR 10dB, $f_{D,\,VC}$=100Hz, $f_{D,\,target}$=600Hz)

Algorithms process matrix of complex samples. Each algorithm is programmed as a function with input and output arguments. Given inputs are matrix of complex samples, PRF, $\sigma_{threshold}$ and known Doppler frequencies (clutter,

target or both). Algorithms' outputs are mean estimated Doppler frequency $\hat{f}_d$ in resolution cell, estimation error, standard deviation of estimates within resolution cell $\sigma_{\hat{f}_D}$ and information if was clutter detected.

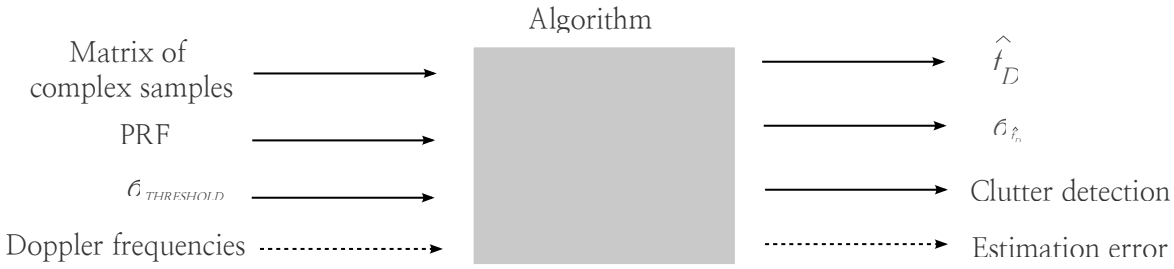

Figure 5.2: Principal inputs and outputs of used algorithms

5.1 Target Doppler signal generation

Target Doppler signal is generated as complex sinusoid

$$s_{target}(m) = A\, e^{j(\omega_D m T + \phi)} \tag{5.1}$$

where A is amplitude of the signal, ω_D is angular Doppler frequency, T is sampling period of slow time signal (i.e. PRI) and φ is initial phase.

5.2 Clutter Doppler signal generation

Clutter Doppler signal is generated in similar fashion as target Doppler signal. Vector of samples of complex sinusoids are formed into array in a way that each Doppler signal begins with random initial phase (one random initial phase for one range bin). Therefore we form cluster of complex samples representing more or less uniform volume clutter.

5.3 Noise generation

Noise is generated as complex noise with normal distribution. Lets assume noise amplitude A_{noise}, R and I are normal random vectors, then vector of complex noise samples will be

$$Noise(m) = \sqrt{A_{noise}}\, R(m) + j\sqrt{A_{noise}}\, I(m) \tag{5.2}$$

6 | Detection and estimation algorithm

Algorithm presented is based on phase difference of successive Doppler signal samples. Instantaneous angular frequency is the time derivative of the instantaneous phase

$$\omega(t)=\frac{d\phi}{dt}(t) \tag{6.1}$$

Therefore Detection and estimation algorithm is furthermore called in short as "Differentiation". In discrete domain, from known phase difference $\Delta\Psi$ and known sampling interval T_{sa} we can calculate Doppler signal frequency as

$$f_d = \frac{\Delta\psi}{T_{sa}}\frac{1}{2\pi} \quad [\text{Hz}] \tag{6.2}$$

To obtain phase difference I use following procedure. Lets consider two complex samples a and b with phases Ψ_a and Ψ_b and with phase difference

$$\Delta\psi=\psi_b-\psi_a \tag{6.3}$$

Phase difference can be computed by using following formula

$$\Delta\psi=arg(ba^*) \tag{6.4}$$

However in this approach I would have to calculate argument for every pair of samples. It is therefore more computationally efficient to work directly with complex samples' coordinates in complex plane. Consider successive complex Doppler signal samples s_1, s_2 and s_3 represented by their phasors (Fig. 6.2a). In a manner to follow formula 6.4 "differential phasors" are constructed by multiplication (and scaling) of successive Doppler signal samples

$$s_{12}=\frac{s_1\,s_2^*}{|s_1\,s_2^*|} \tag{6.5}$$

Differential phasors (Fig. 6.4b) for whole vector of complex samples are formed. In noise-less case all differential phasors would be identical. In real environment with noise present can be observed differential phasors' statistical properties. Mean and variance of real and imaginary parts are computed. Mean values are then used to form final differential phasor which is then processed by CORDIC algorithm to calculate phase difference $\Delta\Psi$. CORDIC algorithm is used, because its specifically designed for effective machine computing and its easily implemented by shifts and adds [14].

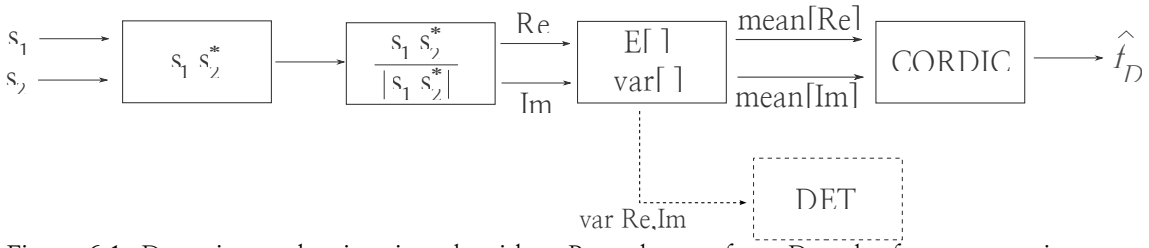

Figure 6.1: Detection and estimation algorithm. Procedure to form Doppler frequency estimate

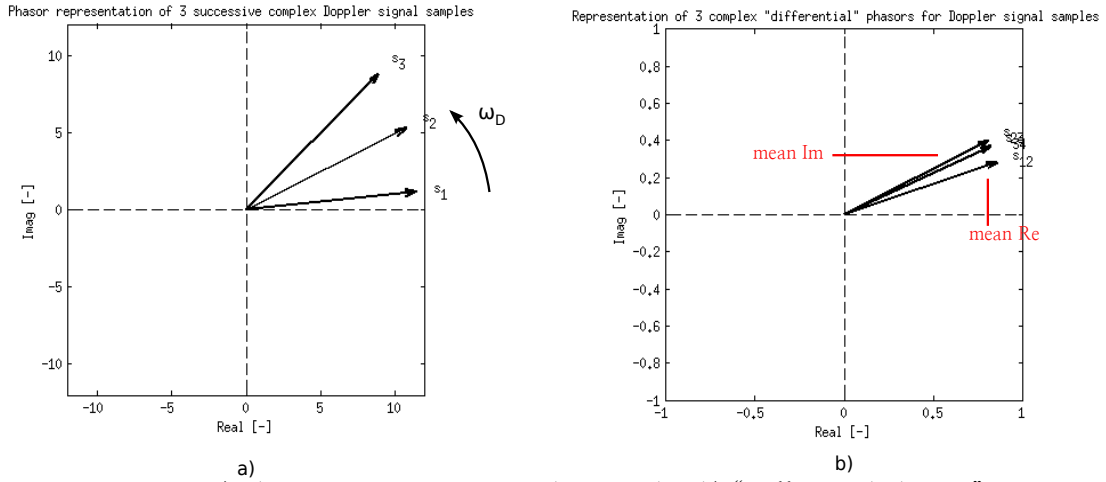

Figure 6.2 a) Phasors representing complex samples, b) "Differential phasors"

Formula 6.2 is used to calculate Doppler frequency estimate $\hat{f}_{D,n}$ for whole vector of samples. Multiple estimates (N vectors in resolution cell) are then compared and mean frequency estimated calculated.

$$\hat{f}_D = E[\hat{f}_{D,n}] \quad \text{for } n = 1, 2, ..., N \tag{6.6}$$

Mean frequency estimate represents estimated Doppler frequency $\hat{f}_d$ of Doppler signal in resolution cell. Standard deviation of frequency estimates is used for clutter detection test.

$$\sigma_{\hat{f}_D} < \sigma_{threshold} \tag{6.7}$$

Threshold test is based on assumption that clutter Doppler signal is more or less uniform in whole resolution cell, thus expected standard deviation of estimated Doppler frequencies is small in comparison to the situation when only noise is present. Same threshold detection test is used for Quadratic Interpolation and Pulse Pair Processing techniques.

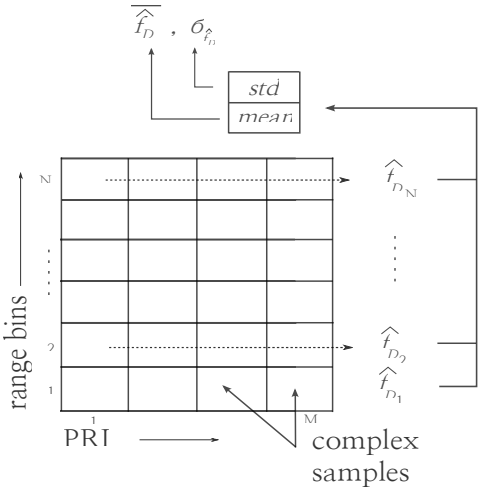

Figure 6.3: Resolution cell and Doppler signal frequency estimate computation

Also must be taken into account variable sampling interval T_{sa}. In modern radar systems are used multiple PRIs to prevent jamming. In our algorithm we have variable T_{sa} in a way that to constant period T is added random suffix ΔT which is 10–20% of T.

7 | Quadratic interpolation around DFT peak

Quadratic interpolation is one of the fine Doppler estimation techniques. Quadratic interpolation around the DFT peak is thoroughly described in [4–Richards] and so we give short notes only.

DFT (or FFT) samples the frequency spectrum and for high resolution we need K (size of DFT) considerably larger than number of signal samples M. If however we have relatively small number of DFT samples our peak in spectrum can differ significantly from the real spectral peak (Fig. 4.7b). Quadratic interpolation takes spectral peak and fits second–order polynomial through the peak and neighbouring two samples. It can be shown that polynomial fit through three samples can be written as [4–Richards]

$$|Y[k_0+\Delta k]|=\frac{1}{2}((\Delta k-1)\Delta k|Y[k_0-1]|-2(\Delta k-1)(\Delta k+1)|Y[k_0]|+(\Delta k+1)\Delta k|Y[K_0+1]|) \quad (7.1)$$

where Δk is distance between peak estimated and peak real (calculated by interpolation). Interpolated peak is then located at $k' = k_0 + \Delta k$, where Δk can be calculated as [Richards]

$$\Delta k=\frac{-(\frac{1}{2})(|Y[k_0+1]|-|Y[k_0-1]|)}{|Y[k_0-1]|-2|Y[k_0]|+|Y[k_0+1]|} \quad (7.2)$$

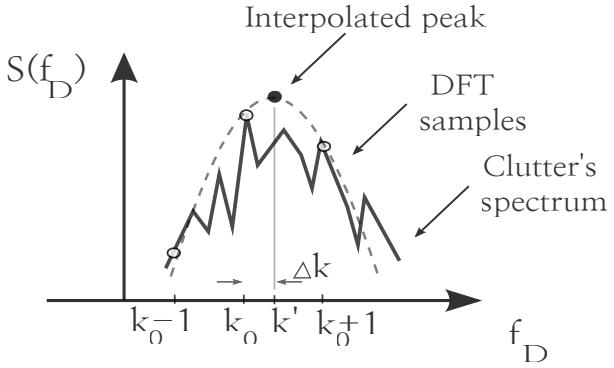

Figure 7.1: Estimated Doppler shift by Quadratic Interpolation

Quadratic interpolation is still effective in high SNR scenarios [4], which is exactly our case with strong volume clutter.

8 | Pulse Pair Processing

Pulse Pair Processing (PPP) is the most advanced technique. It is fully described in [4–Richards]. PPP is widely used in meteorological radars and focuses in volume clutter parameter estimation. PPP works with assumption that one strong Doppler peak and noise is present. Another assumption is that clutter spectrum is approximately Gaussian shaped.

There are time–domain and frequency–domain algorithms. In time–domain algorithm is used for mean frequency estimation autocorrelation function of slow–time data from one range bin. Autocorrelation function of discrete sequence $y[m]$, m=0, ..., $M-1$ is

$$s_y[k]=\sum_{m=0}^{M-k-1} y[m]\,y^*[m+k] \tag{8.1}$$

Lets ignore noise and assume that signal is sinusoid. The first autocorrelation lag then will be (derivation from [4])

$$\begin{aligned} s_y[1] &= \sum_{m=0}^{M-2} y[m]\,y^*[m+1] \\ &= \sum_{m=0}^{M-2} A\,e^{+j2\pi F_0 Tm} A^* e^{-j2\pi F_0 T(m+1)} = |A|^2 \sum_{m=0}^{M-2} e^{-j2\pi F_0} \\ &= |A|^2 e^{-j2\pi F_0} \sum_{m=0}^{M-2} (1) = |A|^2 e^{-j2\pi F_0}(M-1) \end{aligned} \tag{8.2}$$

where argument of exponential is (negative) phase shift between samples of original sinusoid with frequency F_0 Hz. Frequency estimate is then [4]

$$\hat{F}_0=\frac{-1}{2\pi T}\,arg(s_y[1]) \quad \text{Hz} \tag{8.3}$$

It is important to note, and that is why we are using it, that PPP frequency estimator works well for more general signals with adequate SNR [4]. As well it is possible to simplify calculation by just using two following samples.

To estimate spectral variance it is assumed that Doppler spectrum is Gaussian shaped. Firstly volume clutter spectrum is centered at zero Doppler frequency (shift by $\hat{F}_0$) and then we get modified discrete data sequence y'[m]. To obtain spectrum standard deviation we proceed in following fashion (derivation from [Richards]). Autocorrelation function is

$$s_{y'}[k]=|A|^2\,e^{-2\pi^2\sigma_f^2 k^2 T^2} \tag{8.4}$$

The first autocorrelation lag is then

$$s_{y'}[1]=s_{y'}[0]\,e^{-2\pi^2\sigma_f^2 T^2} \tag{8.5}$$

and therefore

$$\sigma_f^2 = \frac{-1}{2\pi T^2} \ln\left(\frac{s_{y'}[1]}{s_{y'}[0]}\right) \quad \mathrm{Hz}^2 \tag{8.6}$$

Natural logarithm can be approximated by series expansion and we get more comfortable expression for spectral width estimator

$$\sigma_f^2 = \frac{-1}{2\pi T^2} \left(1 - \frac{s_{y'}[1]}{s_{y'}[0]}\right) \quad \mathrm{Hz}^2 \tag{8.7}$$

9 | Comparison and performance

In this section detection and estimation algorithm is compared with techniques available in literature[4] and presented above (Quadratic Interpolation around DFT peak, Pulse Pair Processing). All three techniques has been programmed in MATLAB as functions, therefore it's very convenient to simply call and apply them on same data. Each conclusion is based on multiple (hundreds) observations to provide credible results.

Detection and estimation algorithm was designed to be suitable for implementation in DSP. Considering number of resolution cells and their size, other relevant statistical estimators such as Maximum Likelihood (ML) estimator are not suitable.

9.1 Variance of estimates for different methods

Variance of estimates for different methods based on observations is shown on Fig. 9.1. Doppler signal is corrupted by noise and therefore estimation is stochastic process with unpredictable outcome, however we are able to determine statistical properties. From figure it is obvious that estimates are close to Doppler frequency, which is in fact mean value. This variance should be kept in mind while interpreting following results, because presented values will be mean values from multiple observations representing average behaviour.

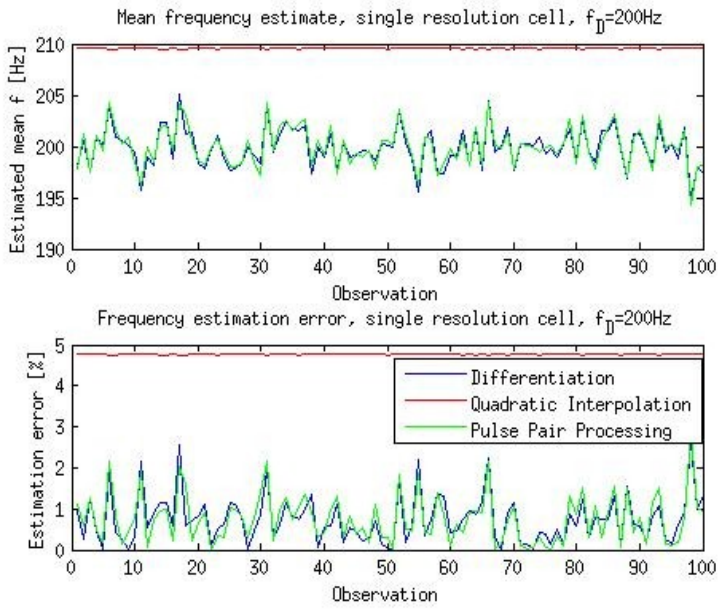

Figure 9.1: Example of variance of estimates for different methods. Single resolution cell filled with clutter Doppler signal and noise. (CNR=20dB, resolution cell size=10x15)

On figure 9.1 are noticeable two trends. Detection and estimation algorithm (Differentiation) and Pulse Pair Processing algorithm give similar results. It is because both algorithms use similar approach in time domain. Pulse Pair

Processing is based on autocorrelation and Detection and estimation algorithm is based on phase difference of successive samples, which in fact, are very similar things. Quadratic Interpolation around DFT peak works in frequency domain, noise has no significant effect on position of spectrum peak, therefore estimates show minimal variance.

9.2 Algorithms comparison based on different SNR

Comparison based on different SNR is the most important analysis. Noise strength is limiting factor in algorithms' performance, therefore the is need to investigate algorithms behaviour and accuracy based on SNR. Analysis will help mee to determine proper use of algorithm and to set up optimal resolution cell size and detection threshold.

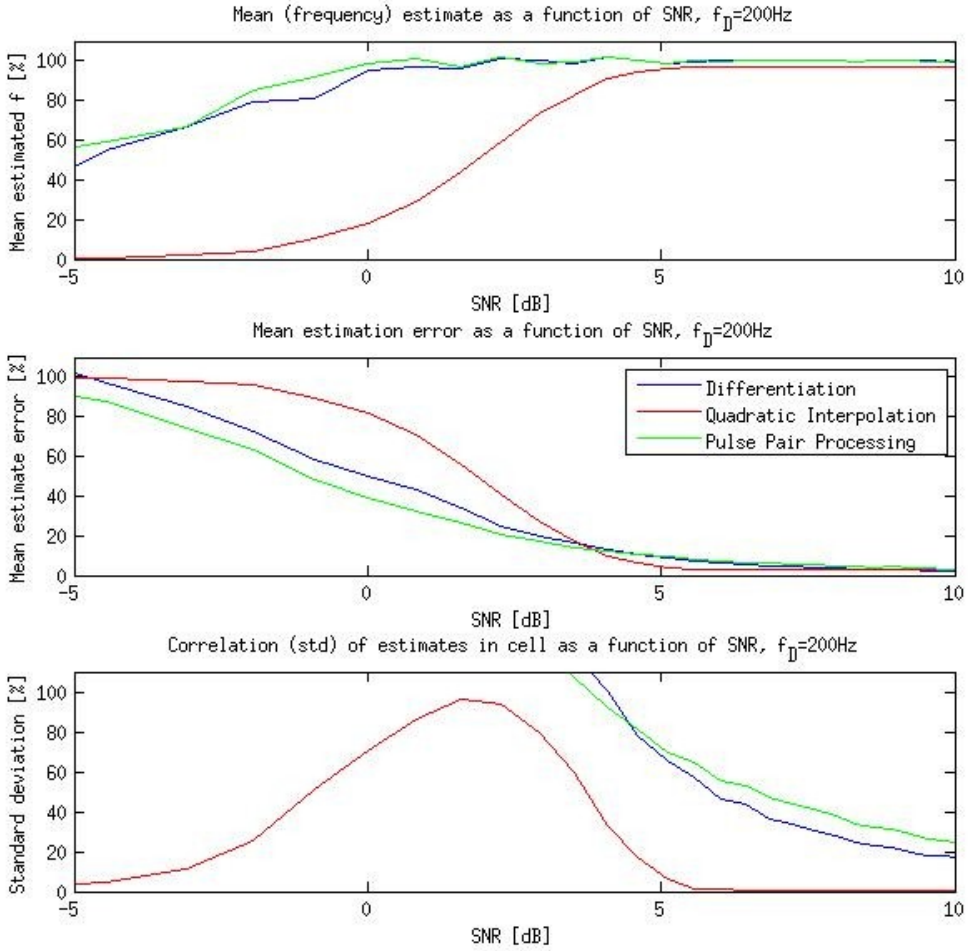

Figure 9.2: Comparison of SNR performance for different methods. (Clutter Doppler frequency=200Hz, resolution cell size=10x15, number of observations = 300)

Results are as expected. Detection and estimation algorithm (Differentiation) and PPP show very similar performance. Estimation error is decreasing with

increasing SNR. Volume clutter signal is typically strong signal, and in Fig.9.2 can be seen that for SNR higher than 3dB mean estimation error is less than 20%. Clutter detection is based on standard deviation of estimates and according to lower graph, standard deviation threshold $\sigma_{threshold}$ should be optimally about 40% (this result will be tested on real data). Behaviour of Quadratic Interpolation around DFT peak algorithm can be divided into tree regions. For low SNR it has zero mean estimated frequency, because clutter signal is too weak and in spectral analysis (FFT) spectrum peak chosen is one of the noise peaks. Therefore for multiple observations mean frequency estimate converges to zero (normal noise distribution). Standard deviation of estimates is low because mean of estimates is near zero repeatedly. In transition region (−2 to 4dB) clutter signal competes with noise, leading to high variance of estimates. In third region is clutter signal significantly stronger than noise and in spectrum is clutter Doppler frequency dominant peak, which is chosen correctly over the most observations, thus leading to low standard deviation.

One of requirements for Detection and estimation algorithm was to be computationally effective and suitable for implementation in DSP. Computational efficiency was compared in MATLAB by measuring processing time needed for each algorithm. For this purpose *tic* [11] function was used. Comparison is illustrative, nevertheless since DSP has different computational architecture than MATLAB, it is expected that our algorithm will in DSP perform even better.

Table 9.1 Average time required for computation [ms].

	Resolution cell size		
	5x8	10x16	15x20
Detection and estimation algorithm	0.81	0.97	1.3
Quadratic Interpolation around DFT peak	0.85	1.2	1.8
Pulse Pair Processing	4.3	7.2	12

Average from 30 000 observations.

9.3 Resolution cell size and SNR analysis

From now on I focus on our Detection and estimation algorithm only. In order to choose optimal size of resolution cell SNR, performance is examined for various cell sizes. Remind two dimensional cell in Fig.9.3. in horizontal dimension are Doppler signal complex samples. Those can be viewed as samples from successive pulses from one range bin (range quanta) or in case of one pulse they can represent different azimuth quanta. In vertical dimension are signal vectors, each of them representing one range bin.

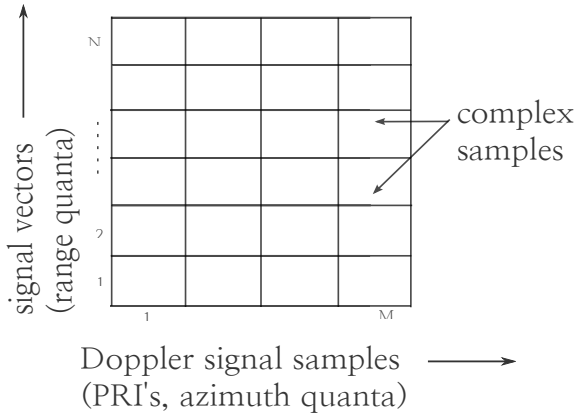

Figure 9.3: Resolution cell size

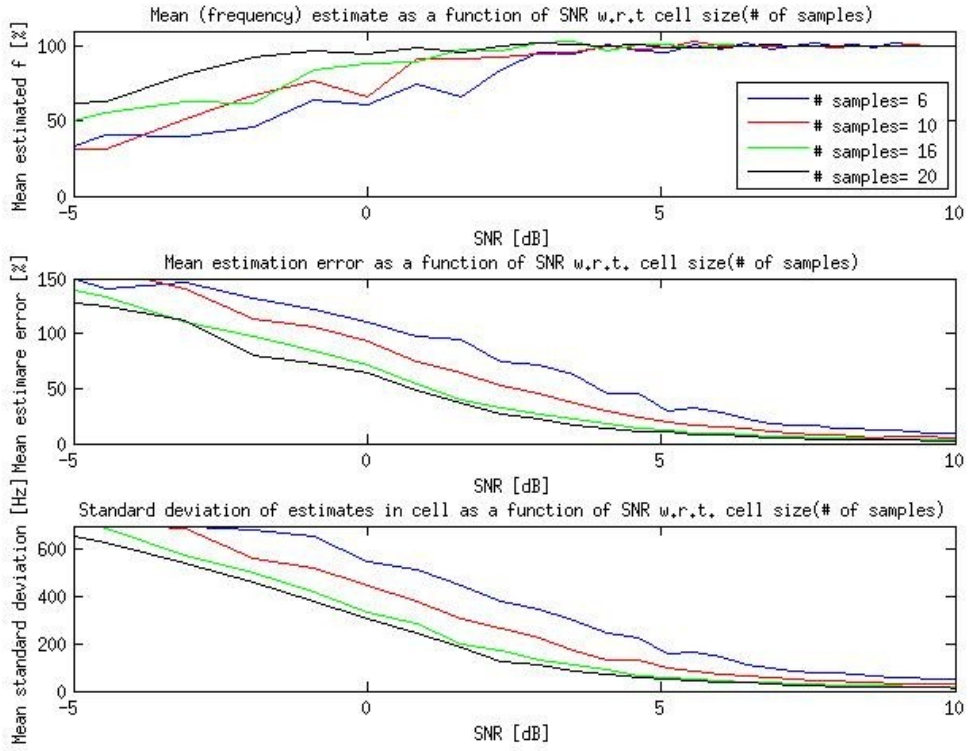

Figure 9.4: Effect of increasing number of Doppler signal complex samples (PRIs) processed. (Clutter Doppler frequency f_D=200Hz, number of signal vectors=10, number of observations=200)

Figure 9.4 shows that with increasing number of processed Doppler signal samples is increasing accuracy of estimation. This result was expected, however significant increase in accuracy is accomplished only if I increase number of samples from six to ten or from ten to sixteen. Improvement in performance while I change number of samples from sixteen to twenty is marginal. This outcome leads to conclusion, that from some point increasing number of samples improves performance only slightly while computational cost is increased

unnecessarily. I can say that accuracy reached "saturation" and optimal size of resolution cell in horizontal domain (i.e. number of Doppler signal complex samples) is around 15.

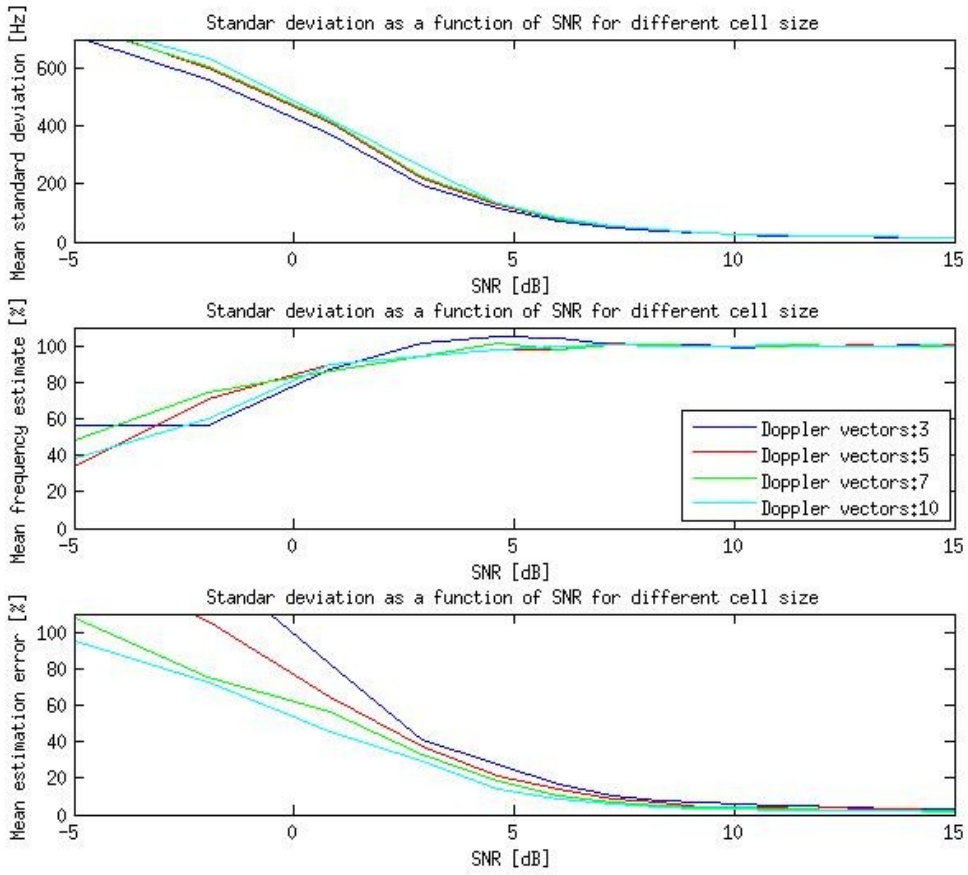

Figure 9.5: Effect of increasing number of Doppler signal vectors processed. (Clutter Doppler frequency f_D=200Hz, number Doppler signal samples=10, number of observations=200)

Figure 9.5 shows that more Doppler signal vectors (more range bins) improve performance only in low SNR region (up to 5dB), however this region is usually out of our interest (clutter signal is usually much stronger than noise). For higher SNR is improvement insignificant. Therefore choice of number of samples vectors in resolution cell is almost arbitrary. Choice is almost arbitrary, because our goal is to have large resolution cell and thus more samples vectors are preferred.

9.4 Performance for different Doppler frequencies

Different clutter Doppler frequencies were put under test.

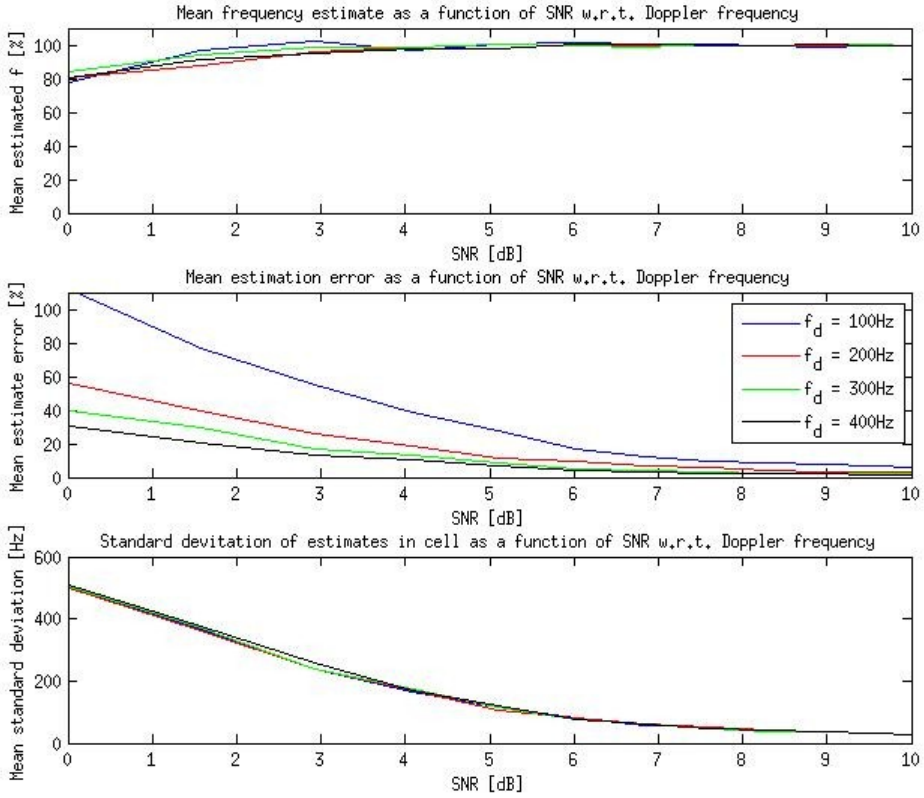

Figure 9.6: SNR performance for different clutter Doppler frequencies

Results show that higher Doppler frequency has lower mean estimate error. However for higher SNR region is difference insignificant.

9.5 Detection performance

For various $\sigma_{threshold}$ was examined percentage of successful detection as a function of SNR. One resolution cell filled with clutter signal and noise underwent detection test. Chosen number of observations was 5000 to obtain statistically relevant results.

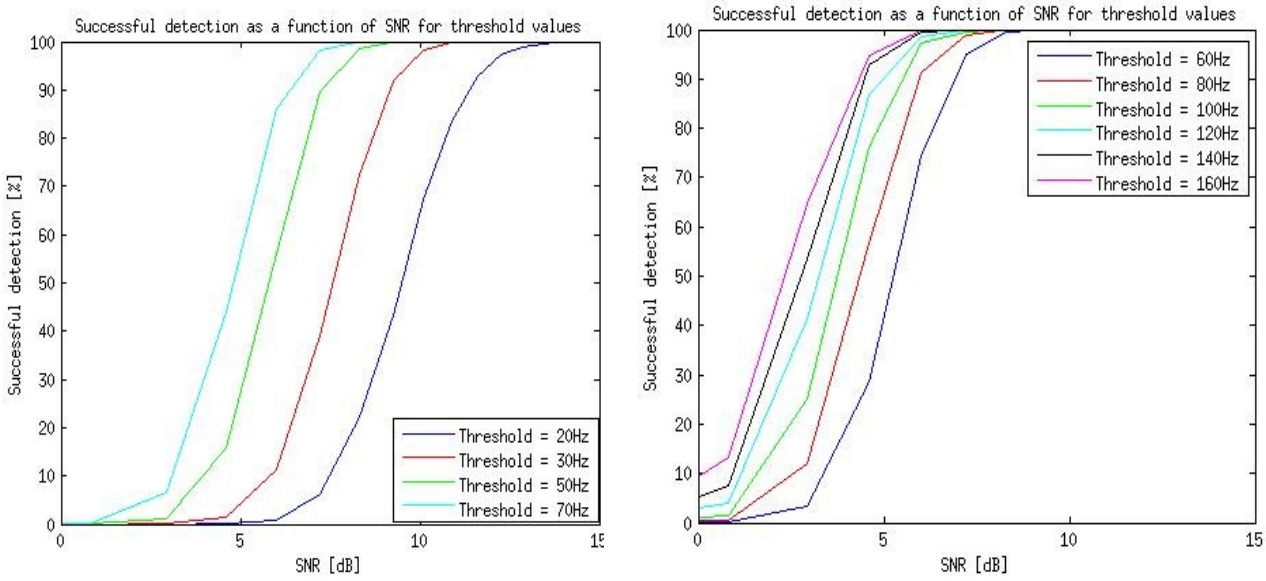

Figure 9.7: Detection performance for various values of $\sigma_{threshold}$. (f_D=200Hz, size of resolution cell=10x15, number of observations= 5000)

Results obtained shows that for low SNR with increasing $\sigma_{threshold}$ is increasing number of successful detections. To prevent, in case of high $\sigma_{threshold}$, false detection while only noise is present, multi-conditional detection test can be implemented. Further condition can be for example that estimated Doppler frequency $\hat{f}_d$ shall not be close to zero. Or to improve detection test, by amplitudes weighted standard deviation can be used.

Another detection scenario is when clutter signal is corrupted by strong target signal. Lets assume one resolution cell filled with volume clutter, noise and one strong target signal as depicted on Fig 9.8.

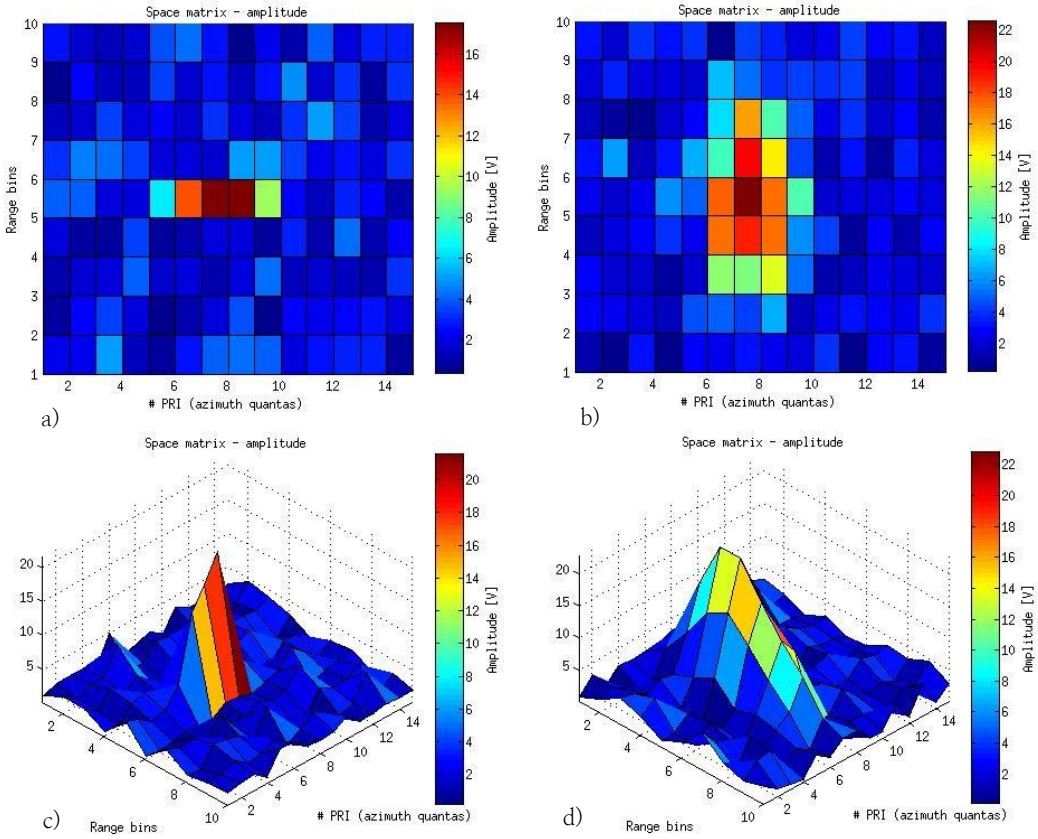

Figure 9.8: One resolution cell with volume clutter signal corrupted by strong target signal in noise background. (CNR=20dB, SCR=20dB, $f_{D,\ clutter}$=200Hz, $f_{D,\ target}$=400Hz, size of resolution cell=9x14)

I examine presence of strong target signal on volume clutter detection. In case when strong target signal is more spacious (Fig. 9.8b) I assume worse detection performance than in case of less spacious (Fig. 9.8a) target signal.

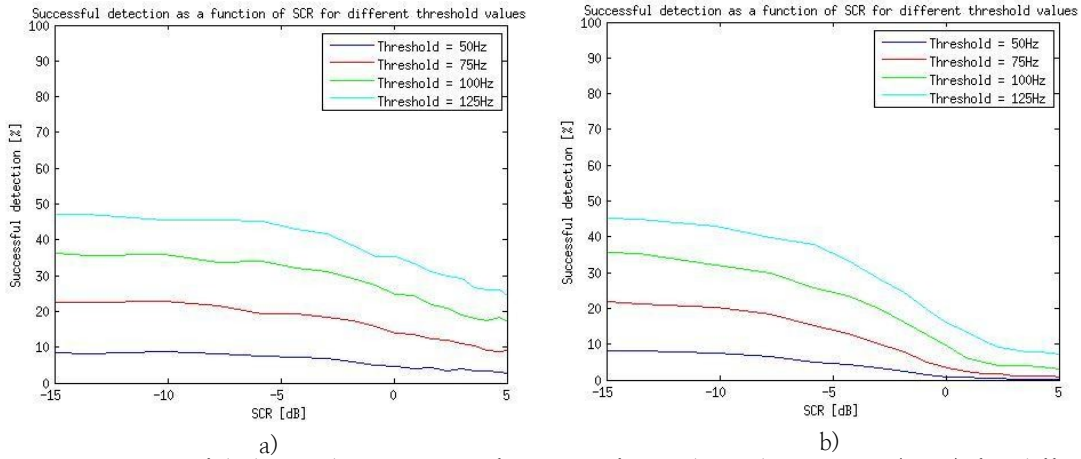

Figure 9.9: Successful clutter detection as a function of Signal to Clutter ratio (SCR) for different detection threshold values. a) with less spacious corrupting target signal b) with more spacious corrupting target signal ($f_{D,\ clutter}$=200Hz, $f_{D,\ target}$=400Hz, size of resolution cell=9x14, number of observations=5000)

With increasing Signal to Clutter ratio (SCR) is successful detection decreasing. Furthermore, detection performance is also determined by number of signal vectors that are corrupted by strong target signal.

10 | Test on real data

Detection and estimation algorithm is tested on radar signal records provided by company RETIA, a.s. [12]. Data provided are matrices of complex envelope samples representing two dimensional space.

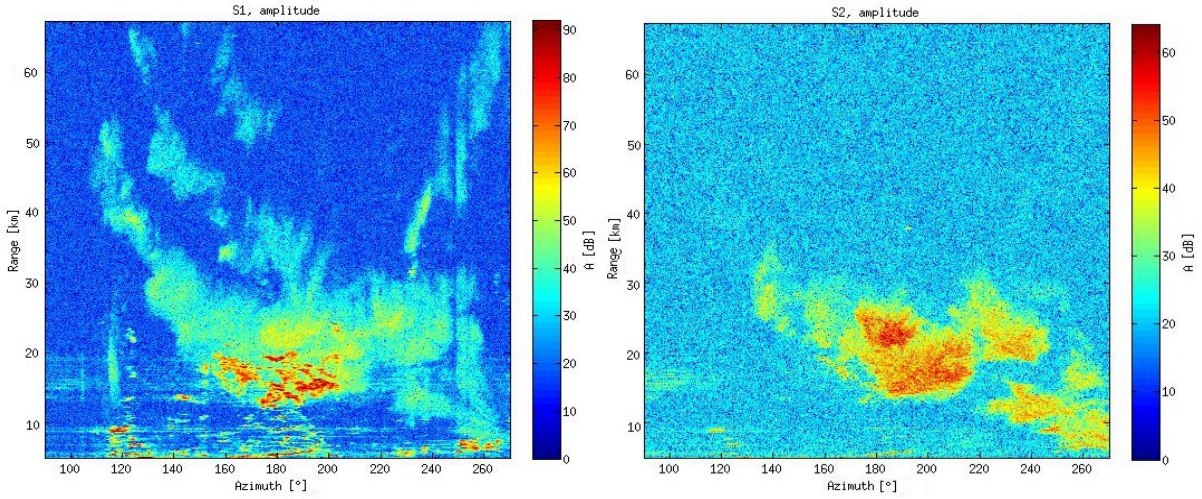

Figure 10.1: Matrices S_1 and S_2 of complex envelope samples representing two dimensional space. Amplitudes of complex samples pictured

Volume clutter is located in areas with high amplitudes. On Fig. 10.1a is present ground clutter as well. Ground clutter is caused by reflections from buildings located in small range and in Fig. 10.2a have ground clutter samples zero phase difference, therefore in Doppler frequencies plot (Fig. 10.3b) they are pictured with zero Doppler frequencies.

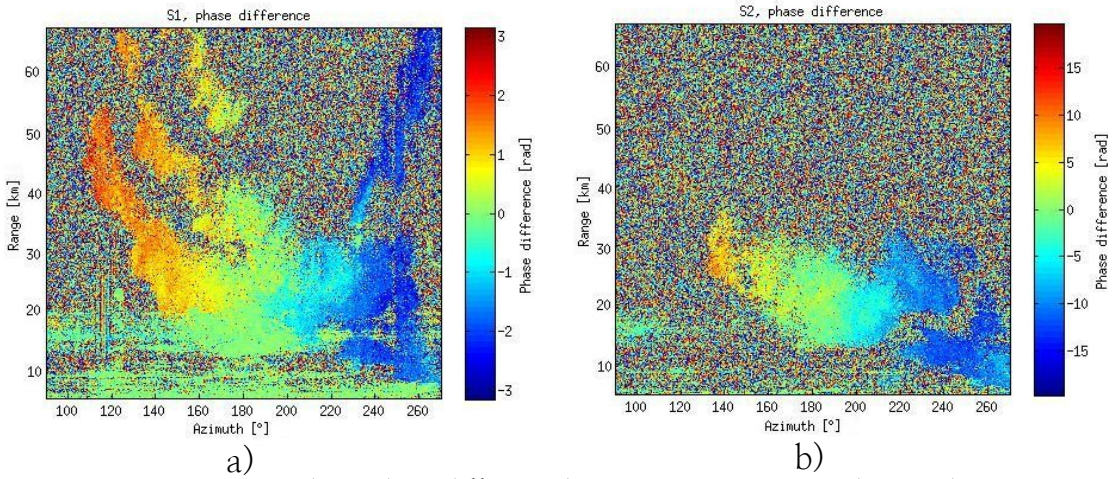

Figure 10.2: Matrices S_1 and S_2 , phase difference between successive complex envelope samples.

Detection and estimation algorithm is tested with various size of resolution cell and for different $\sigma_{threshold}$ to find optimal detection. Detection and estimation algorithm's outputs are detection plot and estimated Doppler frequencies plot.

10.1 Resolution cell size comparison

In this section different sizes of resolution cell are compared. Comparison is done for three different resolution cell sizes: 5x8, 10x15, 15x22 (range x azimuth).

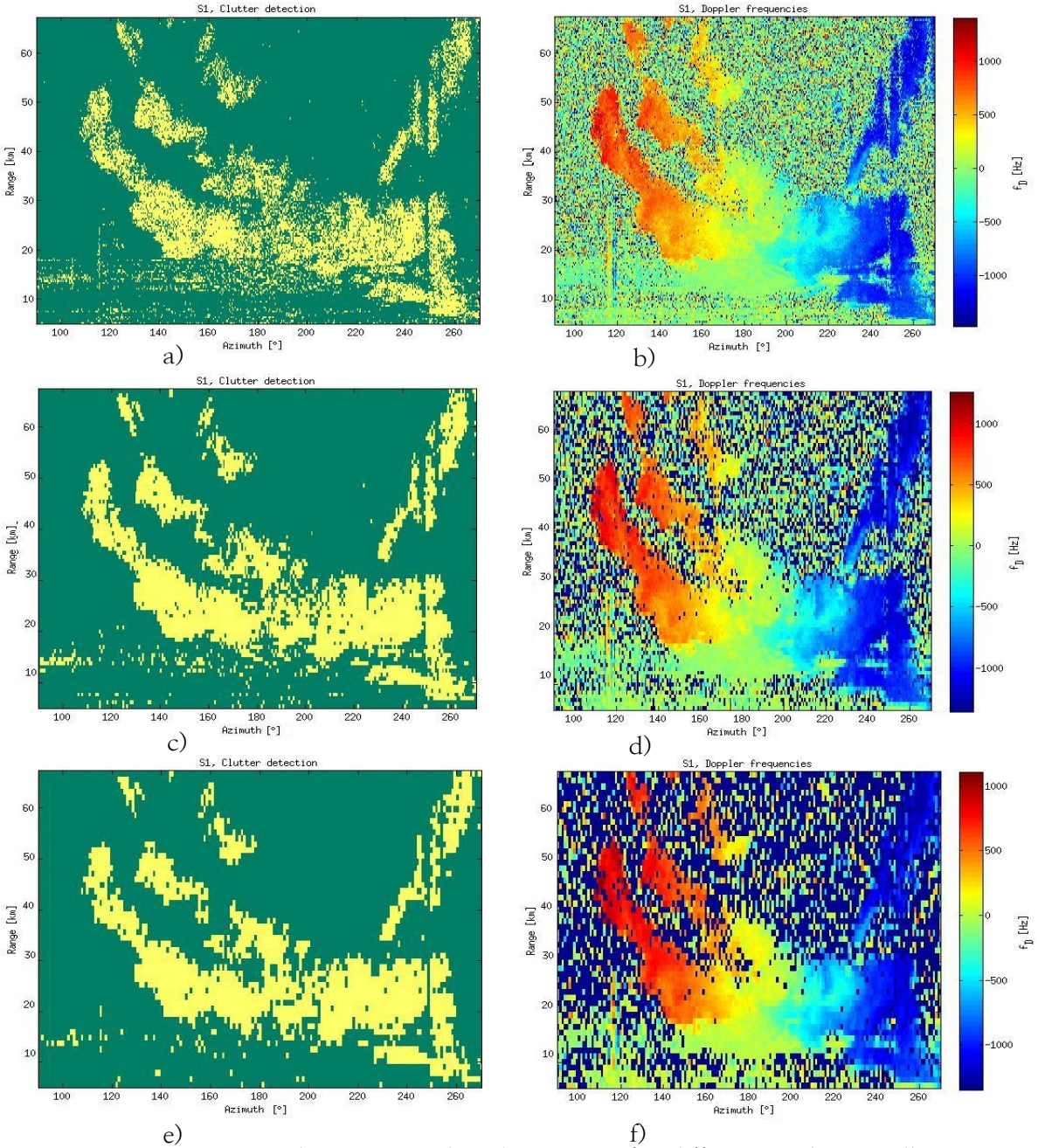

Figure 10.3: Detection and estimation algorithm output for different resolution cell size. S_1 matrix. Top row, resolution cell size = 5x8. Middle row, resolution cell size=10x15. Bottom row, resolution cell size=15x22. (Detection threshold $\sigma_{threshold}$ = 140Hz)

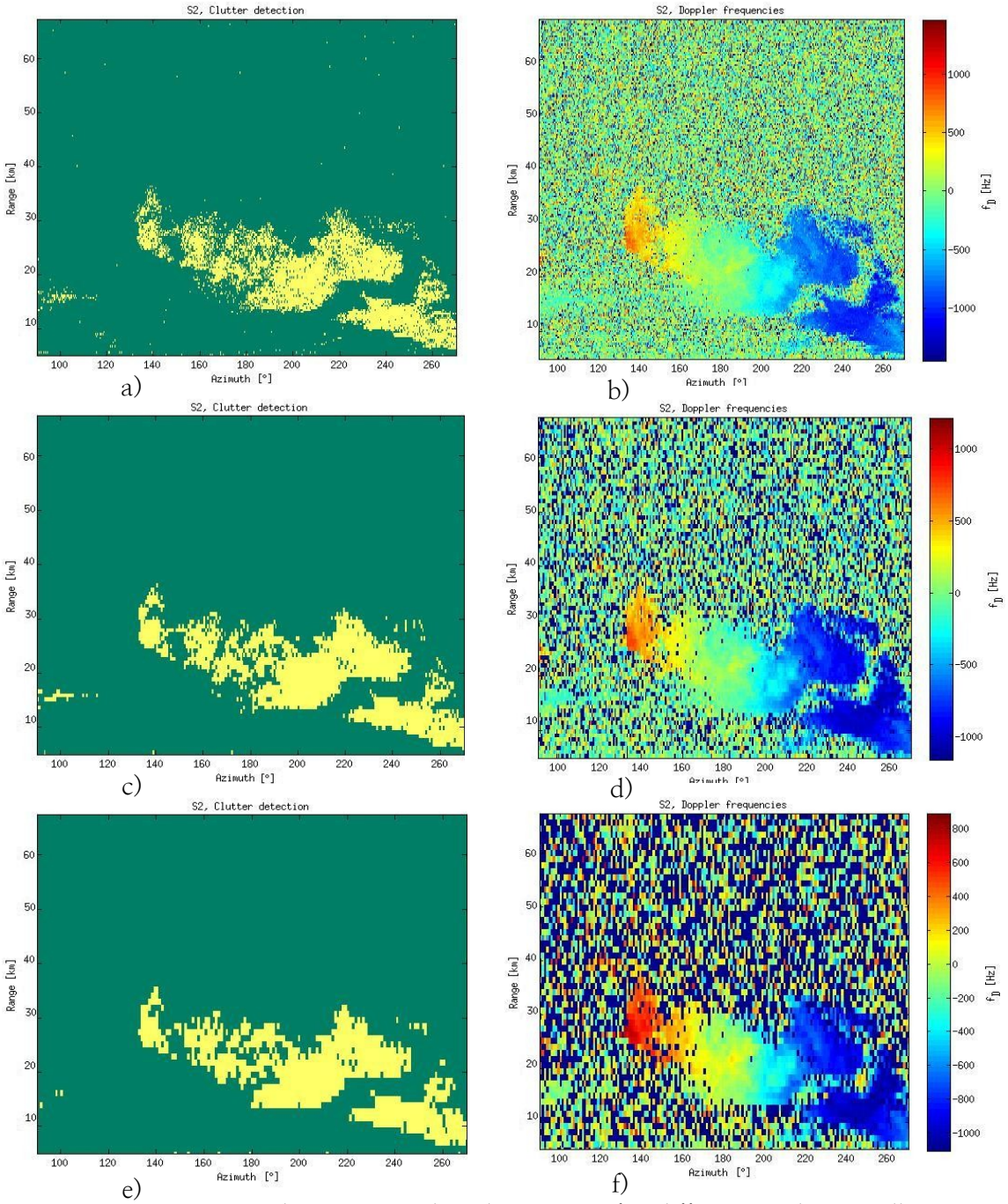

Figure 10.4: Detection and estimation algorithm output for different resolution cell size. S_2 matrix. Top row, resolution cell size = 5x8. Middle row, resolution cell size=10x15. Bottom row, resolution cell size=15x22. (Detection threshold $\sigma_{threshold}$ = 140Hz)

Figures 10.3 and 10.4 show that with smaller resolution cell size more detailed picture of situation is obtained. However smaller resolution cell means as well higher probability of false detection (i.e. noise detected as volume clutter). Another problem is computational cost. As shown on Fig. 10.5 computational cost is exponentially increasing with decreasing size of resolution cell. Therefore optimal trade off for resolution and computational cost has to be decided.

Another requirement is that resolution cell size in range should be in between 500−1000m. Furthermore increasing resolution cell size leads to increase in standard deviation of estimates, because too large resolution cell can contain non−uniform volume clutter. Therefore in our case optimal resolution cell seems to be 10x15.

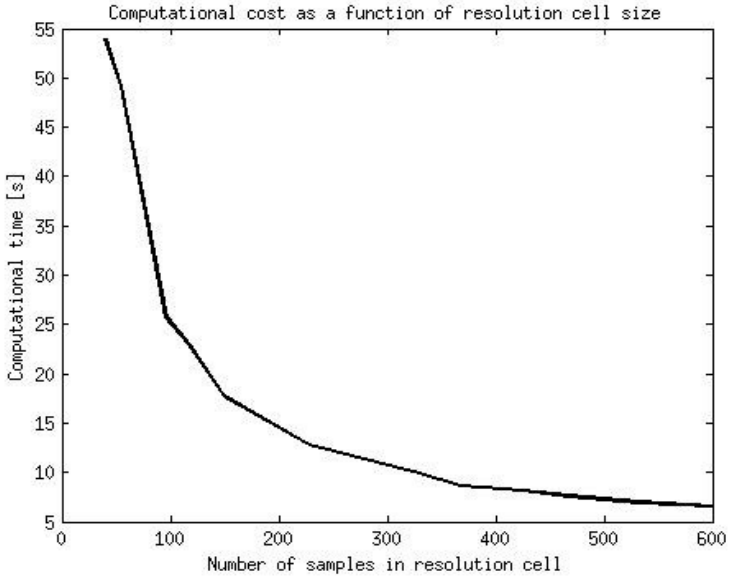

Figure 10.5: Computational cost as a function of resolution cell size(number of samples in resolution cell). (Total number of samples in S_1 matrix is 2964600)

10.2 Detection threshold comparison

In this section different detection thresholds $\sigma_{threshold}$ are compared. Comparison is done for resolution cell size 10x15 and tested $\sigma_{threshold}$ are 60Hz, 80Hz, 100Hz, 120Hz, 140Hz, 160Hz.

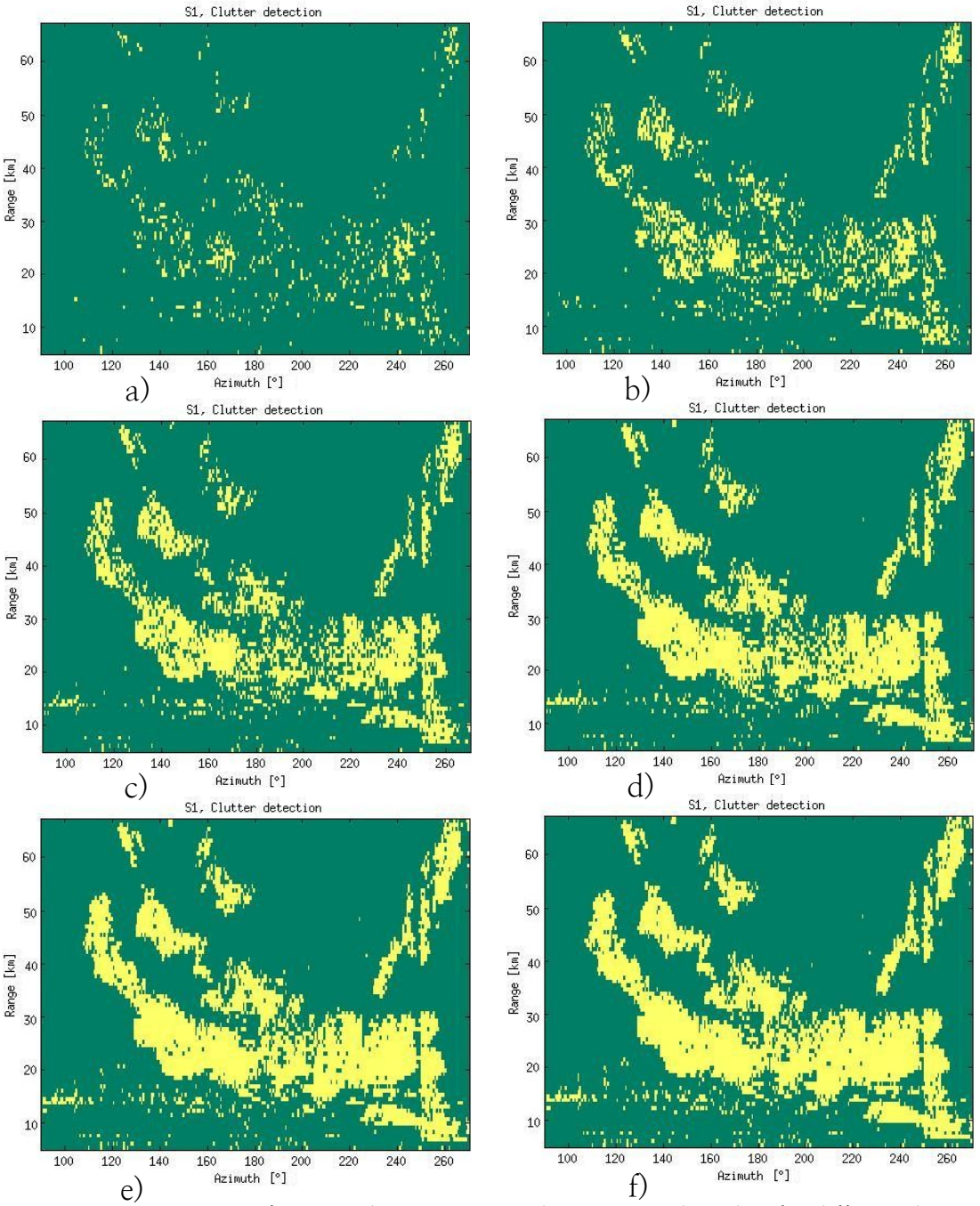

Figure 10.6: Detection performance by Detection and estimation algorithm for different detection thresholds $\sigma_{threshold}$. S_1 matrix. Thresholds are a) 60Hz, b) 80Hz, c) 100Hz, d) 120Hz, e) 140Hz, f) 160Hz. (Resolution cell size = 10x15).

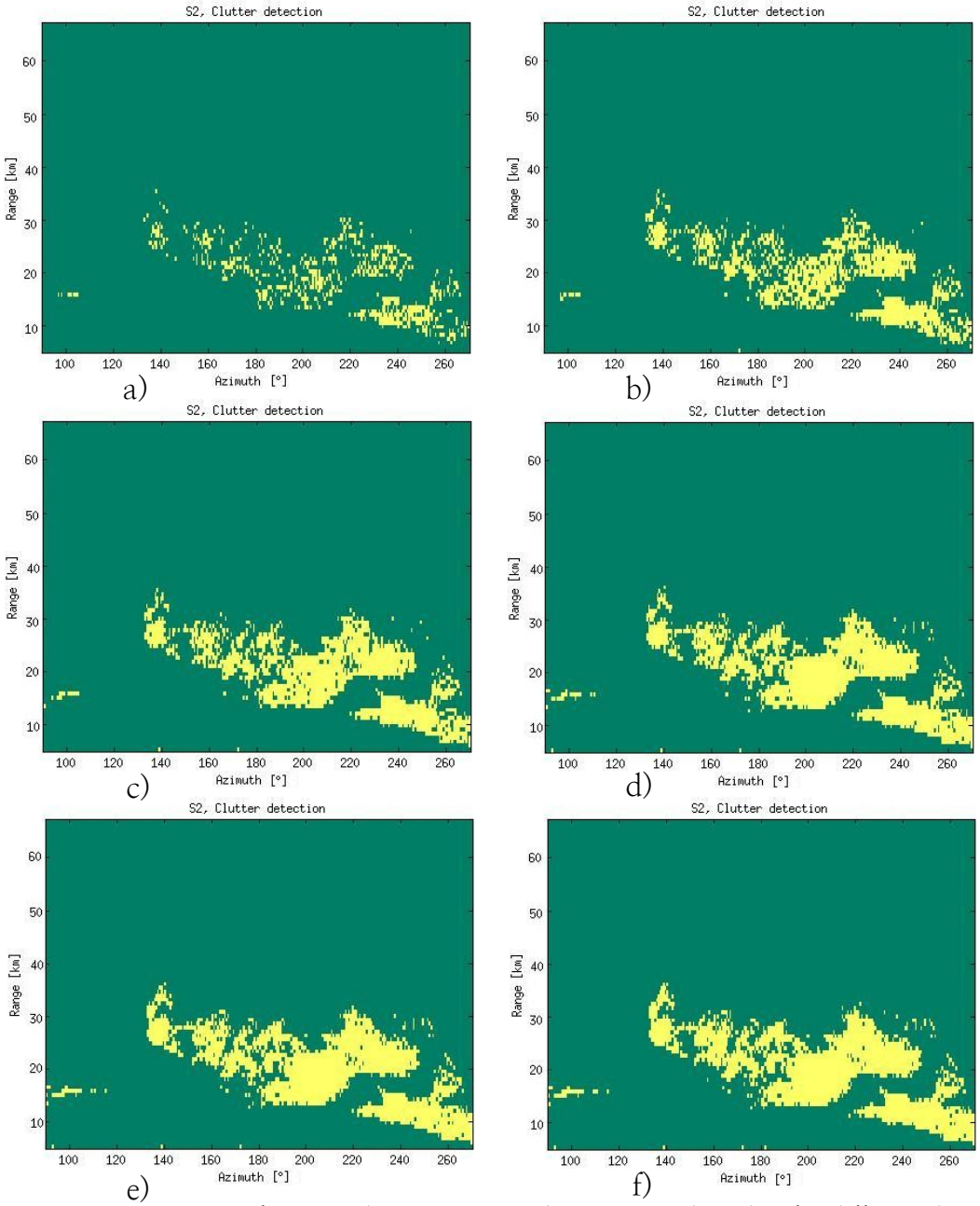

Figure 10.7: Detection performance by Detection and estimation algorithm for different detection thresholds $\sigma_{threshold}$. S_2 matrix. Thresholds are a) 60Hz, b) 80Hz, c) 100Hz, d) 120Hz, e) 140Hz, f) 160Hz. (Resolution cell size = 10x15)

Figures 10.6 and 10.7 shows that with increasing detection threshold $\sigma_{threshold}$ increases probability of volume clutter detection, on the other hand increases probability of false detection due to noise. Higher detection thresholds 140Hz and 160Hz do not increase detection performance significantly (Fig 10.7e,f) and to avoid possible false clutter detection optimal $\sigma_{threshold}$ seems to be around 120Hz.

III Conclusion

Detection and estimation algorithm was designed to allow efficient implementation into DSP. This requirement was fulfilled by clever use of CORDIC algorithm for computing phase of complex sample. Computational efficiency was compared with two algorithms available in literature (Quadratic Interpolation around DFT peak and Pulse Pair Processing). Results show that our algorithm has the smallest computational cost and even better performance is expected since comparison was done in MATLAB, which has different computational architecture than DSP.

Furthermore, I compared algorithms accuracy with respect to different levels of SNR. Detection and estimation algorithm together and PPP have better mean estimation error performance than Quadratic Interpolation around DFT peak. In low SNR region Quadratic Interpolation performs better in standard deviation comparison, however in high SNR region (where we operate) are results for our Detection and estimation algorithm acceptable.

Then I focused on Detection and estimation algorithm's performance with respect to resolution cell size. As expected, an increasing number of Doppler signal samples processed increases estimation accuracy. However, the increase in performance is not linear and "saturation" occurs at 15–20 Doppler signal complex samples, when further increase in complex samples leads only to marginal increase in accuracy. Number of Doppler signal vectors combined has no significant effect in high SNR region. Total number of complex samples in resolution cell determines computational cost. From my analysis is clear that smaller resolution cell leads to finer resolution, but computational cost is increasing exponentially. Requirements are to maximize resolution cell without significant loss in resolution (size of resolution cell in range between 500–1000m). Also resolution cell should not be too large, because with increasing resolution cell increases standard deviation of estimates (larger area means less uniform volume clutter). Therefore optimal size of resolution cell I have chosen 10x15 complex samples.

The choice of clutter Doppler frequency has no significant effect for SNR higher than 6dB. Since the algorithm will operate under high SNR condition, I can conclude that Doppler frequency is irrelevant for the algorithm.

Detection performance analysis reveals that with increasing detection threshold, $\sigma_{threshold}$, the probability of clutter detection increases. Nevertheless it also increases probability of false detection due to noise. Thus optimal $\sigma_{threshold}$ appears to be around 120–140Hz.

One simulation scenario was that target signal was present in resolution cell filled with clutter. The more spacious target signal was, then the more devastating effect it had on clutter detection performance. Strong target signal prevents clutter detection.

Detection and estimation algorithm was tested on real data. Radar signal records provided were matrices of complex envelope samples. Various resolution cell sizes and detection thresholds were examined. Optimal resolution cell size 10x15 predicted by simulations on model appears to be the best choice for processing on real data. Low detection threshold does not detect volume clutter completely. High detection threshold detect volume clutter, but has unwanted side effect of false detections due to noise. Therefore ideal detection threshold around 120–140Hz shows optimal performance as it was predicted by simulation on the model.

Future work can focus on improving detection algorithm. For example weighted standard deviation can be implemented to improve detection in resolution cells, where clutter is present only partially. Furthermore Detection and estimation algorithm can be optimized for non–uniform sampling due to rotating antenna.

Appendix A

A1. Detection and estimation algorithm

```
function[mean_f_est,est_error,VC,std_est]=estimate_diff2(signal,ti,fd,sigma_th)
% Algorithm for mean frequency estimation
%
% Inputs:
%           signal      = Input signal. Vector or matrix
%           ti          = Time sampling vector. Required for difference calc.
%           fd          = Doppler frequency. Required for estimation error calculation [Hz]
%                       sigma_th = Correlation threshold for clutter detection [%].
% Outputs:
%                 mean_f_est = (array) Mean frequency estimate    [Hz] (each angle has 1 estimate)
%                 est_error  = (array) Estimation error. If Doppler frequency known  [Hz] (each angle
                      has 1 est)
%           VC        = Volume clutter present  (yes=1/no=0)
%           std_est   = Correlation (standard deviation) of f estimates
%
% Input signal required to be in form: rows = angles, columns = range bins

%% Errors
% if ~isvector(signal) || ~ismatrix(signal)
% else
%     error('Input signal must be a vector or matrix')
% end

%% Mean frequency estimation

% Equation X.X    <-    s2*conj(s1)/|s2*conj(s1)|
signal_in=(signal(:,2:end).*conj(signal(:,1:end-1)))./(abs(signal(:,2:end).*conj(signal(:,1:end-1))));

% Real and Imaginary coordinates
real_signal=real(signal_in);
imag_signal=imag(signal_in);

% Mean and standard deviation of Re and Im coordinates
mean_r=mean(real_signal,2);
mean_i=mean(imag_signal,2);
std_r=std(real_signal,0,2);
std_i=std(imag_signal,0,2);

% Phase difference
phase_diff=cordic_phase2(mean_r+1i*mean_i);

% Instaneous frequency
Doppler_frequency=phase_diff./(ti(2)-ti(1))*(1/(2*pi));

% Mean frequency estimate
mean_f_est=mean(Doppler_frequency);

% Standard deviation of frequency estimates
std_est=std(Doppler_frequency);

% Frequency estimation error
```

```
est_error=abs(fd-mean_f_est);

%% Clutter detection

noise_th_Hz=40;             % Just noise declared if mean f is in (-Hz,Hz) interval
if mean(mean_f_est) < noise_th_Hz && mean(mean_f_est) > -noise_th_Hz    % If mean f esmated is near 0 ->
noise
   VC=0;
else

      % If correlation (std) between neighbours is high (std low) --> Clutter Present
      if std_est < sigma_th
      VC=1;                    % Volume Clutter present
      else
      VC=0;
      end
end
end
```

A2. Quadratic Interpolation around DFT peak

```
function[mean_f_est_quad,est_error_quad,VC,std_est]=
                =estimate_quad2(signal,fd,N_pulses,N_fft,th,f_PRF,sigma_th)
% Algorithm for mean frequency estimation by Quadratic Interpolation
% Inputs:
%       signal    = Input signal. Vector or matrix
%       fd        = Doppler frequency. Required for estimation error calculation [Hz]
%       N_pulses  = Number of pulses processed
%       N_fft     = Number of fft points
%       th        = Threshold value
%       f_PRF     = Pulse Repetition Frequency [Hz]
%       sigma_th = Correlation threshold for clutter detection
%       std_est  = Correlation (standard deviation) of f  estimates
% Outputs:
%       mean_f_est_quad = Mean frequency estimate by quadratic interpolation    [Hz]
%       est_error_quad  = Estimation error by quadratic interpolation. If Doppler frequency known  [Hz]
%       VC              = Volume clutter present  (yes=1/no=0)
%% Errors
% if ~isvector(signal) || ~ismatrix(signal)
% else
%    error('Input signal must be a vector or matrix')
% end

%------------
%  Algorithm
%------------
% Data signal (rows = angles, columns = range samples)
size_signal=size(signal);

% Init.    (works only for even N_fft)
fs=f_PRF;
f=(0:N_fft-1)*(fs/N_fft);                    % Frequency axis
f_shift=(-1*f(length(f)/2):max(f)/(length(f)+1):f(length(f)/2)); % Freq. axis for fftshift

% Mean f estimation in range-angle cells
for ll=1:size_signal(1);

    % Signal
    signal_data=signal(ll,:);

    % FFT
    fft_data=[];                                    % Reset
    fft_data=fftshift(2*abs(fft(signal_data,N_fft)));          % FFT

    % Threshold test
    counter=0;                      % Reset
    detect_A=[];                    % Initialize arrays
    detect_f=[];
    for k=1:length(fft_data)              % Go through signal spectrum
       if fft_data(k)>=th               % If FFT > th
       counter=counter+1;
       detect_f(counter)=f_shift(k);     % Save f
       detect_A(counter)=fft_data(k);    % Save amplitude
       else
       end
    end
```

```
      % Search for peak
      if length(detect_A) >=1
      peak_power=max(detect_A);                % Maximum in |FFT| for one range-angle cell
      search=find(fft_data==peak_power);       % Find peak
      search2=find(peak_power==detect_A);
      peak_f=detect_f(search2);                % Frequency of peak
      else
      end

      if length(detect_A)>=1             % If is peak > TH, then
         f_peak_est=peak_f;              % Frequency estimation
      else
         f_peak_est=0;                   % Else f est is 0
      end

   if length(detect_A)>=1        % Clutter search if TH was crossed (not empty array)
         k=1;       % Magic constant


    % Quadratic interpolation around the DFT peak (Richards: Fundamentals of Radar Signal Processing p.255)
               if search==length(fft_data) | search==1
                        mean_f_est_quad2(ll)=f_peak_est;
                        est_error_quad(ll)=abs(fd-f_peak_est);
               else
                           deltaK=(-0.5)*(fft_data(search+1)-fft_data(search-1))/abs(fft_data(search-1) -
                                                          -2*fft_data(search)+fft_data(search+1));
            % Mean frequency estimate by Quadratic Interpolation
            f_mean_est_quad=f_peak_est+deltaK;

         mean_f_est_quad2(ll)=k*f_mean_est_quad;              % Mean f. est. matrix
         est_error_quad(ll)=abs(fd-f_mean_est_quad);        % Mean f. est. error matrix

     end
   else
   mean_f_est_quad2(ll)=0;                          % If TH was not crossed, mean f estimate is 0
   est_error_quad(ll)=0;

   end
end

std_est=std(mean_f_est_quad2);
mean_f_est_quad=mean(mean_f_est_quad2);
est_error_quad=abs(fd-mean_f_est_quad);

%% Clutter detection
% If correlation (std) between neighbours is high -> Clutter Present
if std(mean_f_est_quad) < sigma_th
  VC=1;                    % Volume Clutter present
else
  VC=0;
end
end
```

A3. Pulse Pair Processing

```
function[mean_f_est_PPP,est_error_PPP,spectr_width_est,VC,std_est]=estimate_PPP2(signal,fd,f_PRF,sigma_th)
% Algorithm for mean frequency estimation by Pulse Pair Processing
% Inputs:
%       signal    = Input signal. Vector or matrix
%       fd        = Doppler frequency. Required for estimation error calculation [Hz]
%       f_PRF     = Pulse Repetition Frequency [Hz]
%       sigma_th = Correlation threshold for clutter detection
%       std_est  = Correlation (standard deviation) of f  estimates
% Outputs:
%       mean_f_est_PPP  = Mean frequency estimate by Pulse Pair Processing     [Hz]
%       est_error_PPP   = Estimation error by Pulse Pair Processing. If Doppler frequency known  [Hz]
%       spectr_width_est= Spectral width estimate by PPP
%       VC              = Volume clutter present  (yes/no)

%% Errors
% if ~isvector(signal) || ~ismatrix(signal)
% else
%     error('Input signal must be a vector or matrix')
% end

%------------
%  Algorithm
%------------

% Data signal (rows = angles, columns = range samples)
size_signal=size(signal);
% Time axis
fs=f_PRF;
N_pulses=size_signal(2);
ti=(0:(N_pulses-1))/fs;              % Sampling of Doppler signal - Sampling by PRF
 % Mean f estimation in range-angle cells
for ll=1:size_signal(1)
      % Signal
      signal_data=signal(ll,:);

      % Pulse Pair Processing (PPP) method (Richards: Fundamentals of Radar Signal Processing p.266)
          acorr=xcorr(signal_data);                              % Autocorrelation function
          T=1/f_PRF;                                          % Sampling period
          f_mean_est_PPP=1/(2*pi*T)*angle(acorr((length(acorr)+1)/2 +1));  % Mean f estimate by PPP

          k=1;                                                % Magic constant
          mean_f_est_PPP(ll)=k*f_mean_est_PPP;                % Mean f. est. matrix
          est_error_PPP(ll)=abs(fd-f_mean_est_PPP);           % Mean f. est. error matrix

           % Center clutter at zero frequency
           signal_PPP_shift=signal_data.*exp(-1*i*2*pi*f_mean_est_PPP.*ti);
           fft_PPP=fftshift(2*abs(fft(signal_PPP_shift,N_fft)));          % FFT  (for check)

          acorr2=xcorr(signal_PPP_shift);    % Autocorrelation function

          % spectral width estimate  - sigma
          spectr_width_est(ll)=abs(sqrt((-1/(2*pi^2*T^2))*(1-
           (acorr2((length(acorr2)+1)/2)/acorr2((length(acorr2)+1)/2 +1)))));
```

```
end

std_est=std(mean_f_est_PPP);
mean_f_est_PPP=mean(mean_f_est_PPP);
est_error_PPP=abs(fd-mean_f_est_PPP);
spectr_width_est=mean(spectr_width_est);
%% Clutter detection

% If correlation (std) between neighbours is high -> Clutter Present
if std(mean_f_est_PPP) < sigma_th
  VC=1;                    % Volume Clutter present
else
  VC=0;
end

end
```

A4. Target signal generation

```
function[signal]=Target_signal2(A,f,ti,R,N_sa)
% Function to generate complex sinusoid signal
%
% Inputs:      A       - Signal amplitude
%              f       - Signal frequency
%              t       - Time sampling vector
%              R       - Range
%              N_sa    - Number of samples
%
% Outputs:     signal  - Complex sinusoidal Doppler signal

% Signal (complex sinusiod)
target=A*exp(1i*2*pi*f*ti);

% Initial phase
Iph=2*pi*rand(1,length(target));
signal=target+Iph;

signal=signal(1:N_sa);
end
```

A5. CORDIC

```
function[C_angle]=cordic_phase2(c)
% CORDIC for phase computation
% Input:  Complex number
% Output: Phase of complex number [rad]
% Taken and modified from: Krishna 2007
% http://www.dsplog.com/2007/12/16/using-cordic-for-phase-and-magnitude-computation/

if ~isvector(c)
% Complex number for which the phase is  calculated
C_in=c;
else
  for ii=1:length(c)
    C_in(ii)=c(ii);
    [C_angle(ii)]=phase(C_in(ii));
  end
end
end

function[C_in_angle]=phase(C_in)

% Precision required
prec=20;
K=15;                                   % Number of iterations

% % Creating the reference angles - Look up table
% Y_k = ones(prec,1) + j*2.^(-1*[0:1:prec-1])';      % Values of Y
% alpha_k = angle(Y_k);                         % Reference angles, used for finding the cumulative phase
```

```
% Look up table set manually
alpha_k=[0.785398163397448;0.463647609000806;0.244978663126864;0.124354994546761;0.06241880999595
74;0.0312398334302683;0.0156237286204768;0.0078123410601011;0.0039062301319669 7;0.00195312251647
882;0.000976562189559320;0.000488281211194898;0.000244140620149362;0.000122070311893670;6.1035156
1742088e-05;3.05175781155261e-05;1.52587890613158e-05;7.62939453110197e-06;3.81469726560650e-
06;1.90734863281019e-06];

% First rotation - for shifting to first/fourth quadrant
if imag(C_in) <=0
% Rotate by 90 degrees
C_in = -1*imag(C_in) + j*real(C_in);
thetaHat = 1.57079;
else
% Rotate by -90 degrees
C_in = imag(C_in) - j*real(C_in);
thetaHat = -1.57079;
end

% Running for different values of k
for k = 0: K-1

s = -1*sign(imag(C_in)); % Difference
if s == 0 % To handle when sign(imag(C_in)) = 0
s = 1;
end
C_in = C_in.*[1 + s*j*2^(-1*k)];
thetaHat = thetaHat + s*alpha_k(k+1);

% Dumping the variables sign_v(k+1) = s;
thetaHat_v(k+1) = thetaHat;
real_C_in(k+1) = real(C_in);
end

C_in_angle = -1*thetaHat;      % [rad]
end
```

Appendix B

```
%% Velky radar
% Load data
load('20090324-1111_0003.mat')

% Prepare data
S1=rot90(S1,2);
S2=rot90(S2,2);
x_axis=linspace(90,270,3660);              % X, Y axis for plot
y_axis=linspace(2700/1000,64950/1000,830);

%% S1 matrix
% Data, S1 matrix shifted
Sx1=S1(70:899,5493:end);                   % For easier calculations
Sx1(1:830,1833:3660)=S1(70:899,1:1828);    % Cut off calibration signals

% Plot data
figure()                                   % Plot 2D space
imagesc(x_axis,y_axis,20*log10(abs(Sx1))), colorbar, xlabel('Azimuth [Â°]'), ylabel('Range [km]');
title('S1, amplitude'), hb=colorbar(); ylabel(hb,'A [dBLSB]')

% Phase difference plot
S1_phase=angle((Sx1(:,2:end).*conj(Sx1(:,1:end-1))));
figure()
imagesc(x_axis,y_axis,S1_phase),colormap('jet'),colorbar, xlabel('Azimuth quanta'), ylabel('Range quanta');
title('S1, phase difference '), hb=colorbar(); ylabel(hb,'Phase difference [rad]')

% S1 changed
Sx1=Sx1(1:810,:);

% Size of resolution cell  (proccesed resolution)
DR=10;                 % # of range bins
DP=15;                 % # of PRIs (angle quantas)

% Radar parameters
sigma_th=120;          % Threshold for clutter detection (std < signal_th)
fd=0;                  % Unknown volume clutter Doppler frequency
PRF=3300;              % Pulse Repetition Frequency
ti=(0:(DR-1))/PRF;     % Slow time axes

size_Sx1=size(Sx1);
% % Selec resolution cell
% for rr=1:DR:size_Sx1(1);
% for ph=1:DP:size_Sx1(2);
%
%    % Matrix borders, ensure indices do not jump out of matrix
%    if (rr+DR-1) > size_Sx1(1)
%       if (ph+DP-1) > size_Sx1(2)
%        s=Sx1(rr:size_Sx1(1),ph:size_Sx1(2));
%         [mean_f_est,ee2,VC(rr:size_Sx1(1),ph:size_Sx1(2)),ee3]=estimate_diff2(s,ti,fd,sigma_th);
%         mean_f_est_plot(rr:size_Sx1(1),ph:size_Sx1(2))=mean_f_est;
%       else
%        s=Sx1(rr:size_Sx1(1),ph:ph+DP-1);
```

```
%          [mean_f_est,ee2,VC(rr:size_Sx1(1),ph:ph+DP-1),ee3]=estimate_diff2(s,ti,fd,sigma_th);
%          mean_f_est_plot(rr:size_Sx1(1),ph:ph+DP-1)=mean_f_est;
%        end
%    else
%        if (ph+DP-1) > size_Sx1(2)
%        s=Sx1(rr:rr+DR-1,ph:size_Sx1(2));
%        [mean_f_est,ee2,VC(rr:rr+DR-1,ph:size_Sx1(2)),ee3]=estimate_diff2(s,ti,fd,sigma_th);
%          mean_f_est_plot(rr:rr+DR-1,ph:size_Sx1(2))=mean_f_est;
%        else
%        s=Sx1(rr:rr+DR-1,ph:ph+DP-1);
%        [mean_f_est,ee2,VC(rr:rr+DR-1,ph:ph+DP-1),ee3]=estimate_diff2(s,ti,fd,sigma_th);
%        mean_f_est_plot(rr:rr+DR-1,ph:ph+DP-1)=mean_f_est;
%        end
%    end
%
% end
% end
%
% % Plot clutter detection
% figure()
% imagesc(x_axis,y_axis,VC), xlabel('Azimuth [Â°]'), ylabel('Range [km]');
% title('S1, Clutter detection'), colormap(summer)
%
% % Plot Doppler frequencies
% figure()
% imagesc(x_axis,y_axis,mean_f_est_plot), colorbar, xlabel('Azimuth [Â°]'), ylabel('Range [km]');
% title('S1, Doppler frequencies'),  hb=colorbar(); ylabel(hb,'f_{D} [Hz]')


 %%  S2 matrix
% Data, S2 matrix shifted
Sx2=S2(70:899,5493:end);                    % For easier calculation
Sx2(1:830,1833:3660)=S2(70:899,1:1828);     % Cut off calibration signals

% %Plot data
% figure()                                  % Plot 2D space
% imagesc(x_axis,y_axis,20*log10(abs(Sx2))),colorbar, xlabel('Azimuth [Â°]'), ylabel('Range [km]');
% title('S2, amplitude'), hb=colorbar(); ylabel(hb,'A [dBLSB]')
%
% %Phase difference plot
% S2_phase=angle((Sx2(:,2:end).*conj(Sx2(:,1:end-1))));
% figure()
% imagesc(x_axis,y_axis,S2_phase*2*pi),colormap('jet'),colorbar, xlabel('Azimuth quanta'), ylabel('Range
quanta');
% title('S2, phase difference'), hb=colorbar(); ylabel(hb,'Phase difference [rad]')

%
% size_Sx2=size(Sx2);
% % Selec resolution cell
% for rr=1:DR:size_Sx2(1);
% for ph=1:DP:size_Sx2(2);
%
%    % Matrix borders, ensure indices do not jump out of matrix
%    if (rr+DR-1) > size_Sx2(1)
%        if (ph+DP-1) > size_Sx2(2)
%         s2=Sx2(rr:size_Sx2(1),ph:size_Sx2(2));
```

```
%          [mean_f_est2,ee2,VC2(rr:size_Sx2(1),ph:size_Sx2(2)),ee3]=estimate_diff2(s2,ti,fd,sigma_th);
%          mean_f_est_plot2(rr:size_Sx2(1),ph:size_Sx2(2))=mean_f_est2;
%        else
%         s2=Sx2(rr:size_Sx2(1),ph:ph+DP-1);
%         [mean_f_est2,ee2,VC2(rr:size_Sx2(1),ph:ph+DP-1),ee3]=estimate_diff2(s2,ti,fd,sigma_th);
%         mean_f_est_plot2(rr:size_Sx2(1),ph:ph+DP-1)=mean_f_est2;
%        end
%     else
%        if (ph+DP-1) > size_Sx2(2)
%        s2=Sx2(rr:rr+DR-1,ph:size_Sx2(2));
%        [mean_f_est2,ee2,VC2(rr:rr+DR-1,ph:size_Sx2(2)),ee3]=estimate_diff2(s2,ti,fd,sigma_th);
%          mean_f_est_plot2(rr:rr+DR-1,ph:size_Sx2(2))=mean_f_est2;
%        else
%        s2=Sx2(rr:rr+DR-1,ph:ph+DP-1);
%        [mean_f_est2,ee2,VC2(rr:rr+DR-1,ph:ph+DP-1),ee3]=estimate_diff2(s2,ti,fd,sigma_th);
%        mean_f_est_plot2(rr:rr+DR-1,ph:ph+DP-1)=mean_f_est2;
%        end
%     end
%
% end
% end
%
% % Plot clutter detection
% figure()
% imagesc(x_axis,y_axis,VC2), xlabel('Azimuth [Â°]'), ylabel('Range [km]');
% title('S2, Clutter detection'), colormap(summer)
%
% % Plot Doppler frequencies
% figure()
% imagesc(x_axis,y_axis,mean_f_est_plot2), colorbar, xlabel('Azimuth [Â°]'), ylabel('Range [km]');
% title('S2, Doppler frequencies'), hb=colorbar(); ylabel(hb,'f_{D} [Hz]')
```

Bibliography

[1] Skolnik, M., *Radar Handbook*, 3rd Ed., McGraw-Hill, 2008.

[2] Bezoušek, P., Šedivý, P. Radarová technika, Skripta, ČVUT Praha 2004, ISBN: 80-01-03036-9

[3] Mahafza, B. R., *Radar Systems Analysis and Design using MATLAB*, Chapman & HALL/CRC, 2000, ISBN: 1-58488-182-8.

[4] Richards, M. A., *Fundamentals of Radar Signal Processing*, McGraw Hill 2005, ISBN: 0071444742

[5] Schleher. D. C., *MTI and Pulsed Doppler Radar with MATLAB®*, second edition, Artech House 2010, ISBN13: 978-1-59693-414-6

[6] J. G. Proakis and D. G. Manolakis, *Digital Signal Processing*, 3rd Ed., New York: Macmillan, 1996.

[7] Řezáčová, D., Novák, P., Kašpar, M., Setvák, M., Fyzika oblaků a srážek, Academia Praha, 2007, ISBN: 978-80-200-1505-1

[8] Schlesinger, R, J., *Principles of Electronic Warfare*, Prentice-Hall Space Technology Series, Prentice-Hall, Inc., Englewood Cliffs, NJ, 1961.

[9] "Weather Applications and Products Enabled through Vehicle Infrastructure Integration(VII)." Internet: http://ops.fhwa.dot.gov/publications/viirpt/sec5.htm. April 25, 2007 (November 21, 2012).

[10] Nathanson, F. E., *Radar Design Principles, Signal Processing and the Environment*, 2nd Ed., Mendham, New Jersey, McGraw-Hill, Inc. 1991.

[11] MATLAB: http://www.mathworks.com/help/matlab/ref/tic.html

[12] Retia, a.s. http://www.retia.eu/en/

[13] Balanis, C.A., *Antenna Theory, Analysis and Design*, 3rd Ed., John Wiley & Sons, New Jersey, 2005.

[14] "The CORDIC-Algorithm for Computing a Sine" Internet: http://archive.cnmat.berkeley.edu/~norbert/cordic/node4.html